

Mimicking-Bench: A Benchmark for Generalizable Humanoid-Scene Interaction Learning via Human Mimicking

Yun Liu^{*,1,2,3,4}, Bowen Yang^{*,1,2}, Licheng Zhong^{*,3}, He Wang^{2,5}, Li Yi^{†,1,3,4}

¹Tsinghua University ²Galbot ³Shanghai Qi Zhi Institute

⁴Shanghai Artificial Intelligence Laboratory ⁵Peking University

<https://mimicking-bench.github.io/>

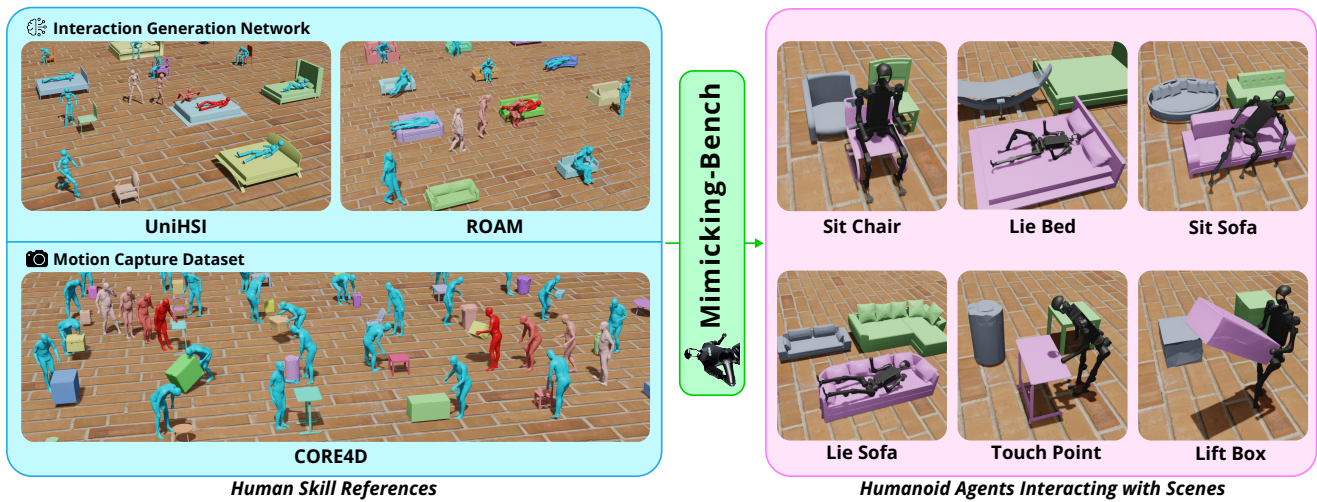


Figure 1. **Mimicking-Bench** is the first benchmark for learning generalizable humanoid-scene interaction skills via mimicking human data, comprising six household interaction tasks. It integrates a diverse human skill reference dataset by leveraging the advances in motion capture dataset and interaction generation network, and constructs a skill-learning paradigm for human-to-humanoid knowledge transfer.

Abstract

Learning generic skills for humanoid robots interacting with 3D scenes by mimicking human data is a key research challenge with significant implications for robotics and real-world applications. However, existing methodologies and benchmarks are constrained by the use of small-scale, manually collected demonstrations, lacking the general dataset and benchmark support necessary to explore scene geometry generalization effectively. To address this gap, we introduce *Mimicking-Bench*, the first comprehensive benchmark designed for generalizable humanoid-scene interaction learning through mimicking large-scale human animation references. *Mimicking-Bench* includes six household full-body humanoid-scene interaction tasks, covering 11K diverse object shapes, along with 20K synthetic and 3K

real-world human interaction skill references. We construct a complete humanoid skill learning pipeline and benchmark approaches for motion retargeting, motion tracking, imitation learning, and their various combinations. Extensive experiments highlight the value of human mimicking for skill learning, revealing key challenges and research directions.

1. Introduction

The past decade has seen remarkable advancements in humanoid robotics [22, 23, 99] and the development of skill learning algorithms for physical simulation environments [93, 126] as well as real-world deployments [11, 29, 57, 68, 85, 131]. For instance, humanoids can now generalize walking skills across a variety of previously unseen terrains by leveraging diverse training data [81]. Meanwhile, there have been significant strides in robot manipula-

*Equal contribution.

†Corresponding author.

tion skills [18, 69, 119], and the emerging task of learning generalizable humanoid skills for interacting with complex scenes is gaining traction. This is a critical step forward for deploying humanoids in real-world scenarios, where they can assist in tasks traditionally requiring human intervention, thereby reducing labor costs and enhancing efficiency.

Due to the complex dynamics of humanoid robots, applying reinforcement learning [30, 84] to explore environments from scratch presents significant challenges in learning generalizable interaction skills that can adapt to a wide variety of scene and object geometries. A promising alternative leverages the topological similarities between humanoid and human skeletons, using versatile human skill data as a rich source of knowledge and guiding humanoids to mimic these skills [24, 35]. While intuitive, this approach faces several technical hurdles, including addressing the discrepancies between humanoid and human models, translating skill animations into executable humanoid control signals, and deriving generalized policies from a diverse set of skill references. Previous works [24, 35, 117] have tackled parts of these challenges, but they are limited to specific interaction scenarios due to the high costs of real-world robot hardware. As a result, there is a growing demand for comprehensive benchmarks [41, 72, 116, 130] that provide standardized platforms for comparing various algorithms and promoting collaborative research. However, existing benchmarks for humanoid-scene interactions either exclude the use of human knowledge [87] or focus on small-scale, specific demonstrations collected through expensive teleoperation [15], making it hard to conduct systematic studies on mimicking a diverse set of human skill references.

To fill this research gap, we present Mimicking-Bench, the first benchmark for generalizable humanoid-scene interaction learning through the mimicking of large-scale, diverse human skill references. Mimicking-Bench spans six household tasks involving whole-body contact scenarios. Constructing Mimicking-Bench addresses two key challenges: first, how to collect a diverse set of human skill references that cover interactions with a wide range of object geometries; and second, identifying which technical aspects within this paradigm warrant further investigation and development. Benefiting from versatile human-scene interaction datasets [33, 44, 118] and derived interaction generation networks [108, 122, 124] in the fields of computer vision and graphics, we address the first challenge by integrating both real-world and automatically synthesized human-scene interaction data. This comprehensive skill knowledge source encompasses 23K human-scene interaction motion sequences, covering 11K diverse object geometries. To address the second challenge, we investigate various existing human mimicking pipelines [24, 35, 93, 96] and identify three successive core technical modules: 1) retargeting human motions to humanoid skeletons [35, 56], 2) tracking

skill animations in physical simulation environments [37, 96], and 3) imitating humanoid skill demonstrations [16, 58, 129]. By connecting these modules, Mimicking-Bench constructs a general skill-learning paradigm that encompasses different existing pipelines. With a wide array of algorithms available for each module, Mimicking-Bench enables two types of studies: 1) comparing existing, well-established humanoid skill learning pipelines [24, 35], and 2) evaluating various outstanding modular algorithms, promoting comprehensive research on all key techniques involved in humanoid-scene interaction learning.

Extensive experiments are conducted through pipeline-wise and module-wise method comparisons, highlighting the critical importance of selecting the appropriate algorithms for each module. By integrating the best algorithm for each module, the approach of mimicking human references results in more natural motion generation and significantly improves task success rates compared to data-free reinforcement learning. These results demonstrate the effectiveness of human mimicking in humanoid-scene interaction learning and its potential to advance the field.

In summary, our main contributions are fourfold: 1) We present Mimicking-Bench, the first comprehensive benchmark for generalizable humanoid-scene interaction learning via human mimicking. 2) We integrate a large-scale and diverse human skill reference dataset that encompasses both synthesized and real-world human-scene interactions. 3) We develop a general skill-learning paradigm and provide support for both pipeline-wise and modular evaluations. 4) Extensive experiments validate the effectiveness of the human mimicking paradigm and reveal new challenges and research opportunities for future exploration.

2. Related Work

2.1. Benchmarks for Humanoid Skill Learning

Early works [28, 38, 41, 43, 67, 72, 116, 130] have benchmarked robot-object interaction skill learning on dexterous hands [53] and robot arms [2]. Driven by rapid progress in humanoid robot models [23, 51, 99] and skills [81, 117, 119] in both simulation and real-world scenarios, various benchmarks for humanoid robots have been developed to explore the capabilities of diverse skill learning methods in a scalable and reproducible manner. Table 1 provides a brief summary of these benchmarks. For humanoid skill learning, one branch of benchmarks [5, 8, 94] focuses on humanoid locomotion skills such as walking, running, and stabilization. Another emerging branch aims to foster studies on humanoid-scene interactions [15, 87], where HumanoidBench [87] supports demonstration-free reinforcement learning (RL), and BiGym [15] collects a small set of demonstrations via manual teleoperation for benchmarking imitation learning methods. However, these

benchmarks are limited by the restricted generalizability of RL algorithms and the small scale of demonstrations due to the high cost of teleoperation. They cannot assess a method’s ability to generalize across scene and object geometry changes, nor can they support studies on human-to-humanoid skill transfer. In contrast, Mimicking-Bench presents a comprehensive solution by enabling learning from large-scale, diverse human skill references, benchmarking popular algorithms for each core technical module, and supporting research on generalization with diverse object geometries.

2.2. Human-Scene Interaction Dataset and Motion Generation

Capturing [92, 109–111] and synthesizing [52, 54] human-scene and human-object interactions are key tasks in the computer vision and graphics communities. Various dataset initiatives have been launched to collect real-world human motions interacting with static 3D scenes [32, 33, 44, 121], dynamic objects [7, 39, 120, 125, 128], and human collaborators [59, 106, 118], while a recent work [6] explores the collection of synthetic interaction data using VR devices. Supported by these datasets, a variety of motion generation techniques have emerged, each with a different focus. One branch of works [45, 52, 90, 122, 123] treats fixed static scenes as inputs and focuses on generating human motions only, while another branch [19, 54, 55, 75, 113] generates motions for both humans and movable objects simultaneously. With the rapid progress in large language models (LLMs) [4], recent works [105, 108, 114] have unlocked long-range interaction generation abilities by designing LLM planners. By leveraging these advancements, we construct a large-scale, versatile dataset of human-scene interaction skill references and establish a bridge between motion generation techniques and humanoid skill learning.

2.3. Humanoid Imitation Learning

As a key technical module for humanoids mimicking humans, humanoid imitation learning has been a long-standing research topic aimed at enhancing humanoid skill learning through demonstrations. Considerable progress has been made in various areas, including humanoid locomotion [17, 20, 62, 78, 81, 82, 93, 95, 102], humanoid-object interaction [24, 69, 73, 96, 104, 108], and multi-agent collaboration [26, 63]. In the context of direct solutions, single-stage approaches [15, 81, 96] use a single policy network to generate actions, where motion discriminators [27], which encode prior knowledge from demonstrations, are incorporated in some works [17, 26, 34, 63, 73, 77, 82, 93, 102, 108] to further improve the naturalness of humanoid motions.

To enable the reuse of learned skills for unseen

tasks [78], two-stage methods [24, 95, 104] decompose task fulfillment into two parts: first, planning key motion objectives (such as target joint positions [24], motion semantics [104], or learnable motion features [20, 49, 62, 69, 78, 95]), and then controlling the humanoid to complete them. These methods assign the planning and control tasks to a high-level planner and a low-level controller, respectively.

3. Mimicking-Bench

We contribute Mimicking-Bench, a new benchmark for human-to-humanoid generalizable interaction skill transfer, encompassing 6 humanoid-scene interaction tasks spanning 11.8K diverse object shapes and 25K human references. We first introduce the simulation environment configurations of Mimicking-Bench in Section 3.1. We then provide formulations and evaluation metrics for our six humanoid-scene interaction tasks in Section 3.2. Finally, to facilitate learning from human data, we present the methods for human skill reference collection for each task in Section 3.3.

3.1. Simulation Environment

As shown in Figure 2 (a), Mimicking-Bench is constructed in the Isaac Gym [65] simulation environment. The humanoid robot used in the benchmark is the Unitree H1 [99], consisting of 19 revolute joints. The physical model of the H1 follows the Unitree public implementation [100] for Isaac Gym. Below, we describe the key design elements, with additional details in the supplementary.

Observations. We draw inspiration from recent advancements in real-world vision-based humanoid control [24, 35] and develop an egocentric visual perception system for the humanoid. To gather information from all directions around the humanoid body, we attach four egocentric cameras to the humanoid’s root link, each with a 120-degree field of view, as shown in Figure 2 (c). These cameras provide panoramic coverage, enabling the humanoid to interact with objects from any direction. The **visual observations** of the humanoid include color images \mathcal{C} , depth images \mathcal{D} , and semantic segmentation maps \mathcal{S} from the four cameras, combined with an elevation map \mathcal{E} [42, 70] shown in Figure 2 (b). The elevation map is generated by merging depth images into the humanoid’s root coordinate system and projecting them onto the ground. In addition, the humanoid’s **proprioception** s_{prop} consists of 19 degrees of freedom (DoF) joint angles, 19 DoF joint velocities, and 2 DoF for the gravity direction at the humanoid’s root. Combining all the sensory inputs, the complete observation space is defined as $\mathcal{O} = \{s_{\text{prop}}, \mathcal{C}, \mathcal{D}, \mathcal{S}, \mathcal{E}\}$.

Actions. Mimicking-Bench supports position, velocity, and torque control, all of which operate in 19-dimensional action spaces with a control frequency of 50 Hz. For both position and velocity controls, we employ a PD controller, using the same proportional-derivative gains as those in Hu-

Benchmark	Characteristics:				Benchmark Aspects:			# Number of:		
	Bipedal	Interaction	Generalization	Human Reference	Retargeting	Tracking	Imitation Learning	Human Reference	Object	Task
<i>Plappert et al.</i> [79]		✓						-	3	4
MetaWorld [116]		✓						-	66	50
RLBench [41]		✓					✓	-	302	106
RoboSuite [130]		✓						-	23	9
FurnitureBench [38]		✓						-	8	8
D3IL [43]		✓						-	19	7
ManiSkill [72]		✓		✓				-	162	4
ManiSkill2 [28]		✓		✓				-	2.0K	20
Gym-Mujoco [8]	✓							-	0	2
<i>Tassa et al.</i> [94]	✓							-	0	6
LocoMujoco [5]	✓							0.9K	3	27
HumanoidBench [87]	✓	✓		✓				-	28	27
BiGym [15]	✓	✓					✓	-	71	40
Mimicking-Bench	✓	✓	✓	✓	✓	✓	✓	23.4K	10.6K	6

Table 1. Comparison of Mimicking-Bench with existing robotic skill learning benchmarks.

manPlus [24]. In our experiments, we use position control due to its universality and to ensure consistency with existing real-world implementations [24, 35, 119].

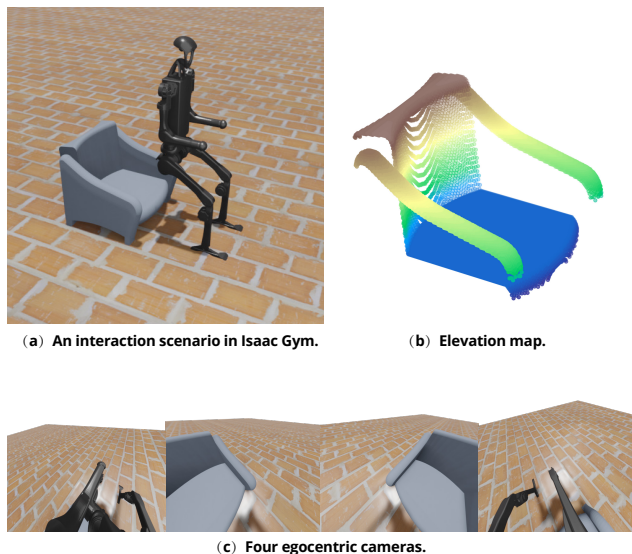


Figure 2. **Mimicking-Bench simulation configurations.** (a) exemplifies an interaction scenario of H1 in Isaac Gym. (b) and (c) show the captured elevation map and color images from four egocentric cameras.

3.2. Task Formulations and Evaluations

Aiming to bridge the gap between graphical human interaction synthesis methods [46, 91, 108, 122, 124] and robotic humanoid skill learning [5, 15, 87], Mimicking-Bench focuses on everyday household human-scene interaction scenarios that are widely studied in the computer vision community. This includes five tasks involving interactions with static scenes and one with dynamic scenes.

Evaluation metrics. To assess whether methods can successfully achieve the tasks and adapt to real-world robots, we propose a combination of kinematic and physical metrics. The kinematic metric K evaluates task-specific key joints of the humanoid to determine whether they meet predefined task goals. The physical metric $P = [\max(\|\tau_i v_i\|^2) < \lambda_P]$ ensures that humanoids perform

movements with sufficiently low energy costs, where i , τ , and v denote the frame index, mean joint torque, and mean joint velocity, respectively. Since the expected values of λ_P for sim-to-real transfer are unknown, we select four values with exponential increments and report the average success rates under these values.

We present brief formulations and kinematic evaluation metrics for each task below. Detailed formulations are provided in the appendix.

(1) Sitting on a Chair (SC). The humanoid must navigate the scene, locate, and stably sit on a fixed unseen chair. The kinematic evaluation ensures that the pelvis of the humanoid remains above the seat surface.

(2) Sitting on a Sofa (SS). The humanoid is required to find and sit steadily on a fixed unseen sofa. Compared to chairs, sofas in our dataset have significantly longer lengths and shorter heights, which lead to different sitting poses and reduce reliance on the seat back. The kinematic evaluation for this task is the same as that for SC.

(3) Lying on a Bed (LB). The humanoid needs to locate, sit, and finally lie on a fixed unseen bed. The kinematic evaluation ensures that both the pelvis and ankles of the humanoid remain on top of the bed.

(4) Lying on a Sofa (LS). The humanoid must locate, sit, and lie on a fixed unseen sofa. Since the humanoid is too large to move its entire body onto the sofa, the kinematic evaluation requires the pelvis to remain on the sofa, while the ankles should be raised to about half the sofa’s height to ensure that support is solely from the sofa.

(5) Touching Points Near an Object (T). In this task, with an unseen household object in the scene, the humanoid must move its wrists to target positions that allow easy manipulation of the object. The target wrist positions are specified by markers on the elevation map, which is used as additional visual input. The kinematic evaluation ensures that the wrists remain near the target positions.

(6) Lifting a Box (L). Given a box of an unseen scale, the humanoid must locate and lift the box to reach a specific height. The kinematic evaluation measures whether the box is above the target height and the hands are attached to the

object by the end of the task.

3.3. Human Skill Reference Collection

Benefiting from advances in understanding and synthesizing human-scene interactions, we have integrated a large-scale human skill reference dataset for the six tasks. The data collection process for each task is described below.

Generating human-scene interaction by UniHSI [108]. For sitting on chairs and lying on beds, we generate reference motions using UniHSI [108], which takes Chains of Contacts as input and outputs humanoid motions for the AMP [77] robot. We apply the policy trained on PartNet [71] scenes, manually generating Chains of Contacts for inference. To enhance diversity, we randomly scale and stretch objects, and vary the robot’s initial position. Only successful interactions are retained.

Generating human-sofa interaction by ROAM [122]. For sitting and lying on sofas, we use ROAM [122] in two stages. First, the goal pose synthesis network generates final sitting poses and matches them to object meshes (from ShapeNet [9]). Multiple sitting poses are assigned to each mesh, with random scaling for diversity. In the second stage, ROAM generates the full motion sequence, simulating a human walking toward the sofa and sitting down. The human’s initial position and orientation are randomly set.

Selecting interaction clips from CORE4D [118]. For the tasks of touching points and lifting boxes, we acquire human skill references from the existing motion capture dataset CORE4D [118]. For the touching points task, we automatically detect the frames where humans are about to touch an object by calculating the hand-object distance and clip the interaction sequences leading up to these frames as human skill references. For the lifting boxes task, we select 30 large boxes and clip the corresponding interaction data based on whether the box reaches the target height.

Dataset statistics. Table 2 presents statistics on the dataset, showcasing a wide variety of objects and skill references, with significant diversity in object scales. By leveraging this dataset, Mimicking-Bench fosters studies on the generalizability of methods to changes in object geometry.

Task	Object				Human Reference	
	Number	Length (cm)	Width (cm)	Height (cm)	Number	Duration (s)
SC	4.6K	57.8(±14.9)	55.6(±15.1)	80.6(±17.6)	5.0K	14.8(±0.5)
SS	1.5K	131.1(±21.1)	63.0(±21.7)	57.3(±21.8)	7.6K	12.1(±0.0)
LB	350	227.3(±42.7)	177.7(±39.4)	85.7(±27.0)	1.6K	24.8(±0.7)
LS	1.8K	191.2(±28.3)	86.7(±25.2)	78.5(±25.7)	6.1K	12.1(±0.0)
T	2.3K	59.6(±19.2)	53.2(±16.2)	56.1(±16.7)	2.3K	3.3(±0.2)
L	30	67.3(±6.4)	43.4(±6.2)	88.9(±7.8)	890	4.3(±0.2)

Table 2. Statistics on human skill references.

4. Skill Learning Paradigm

Learning humanoid skills from human data is an emerging field [24, 34, 35, 61], supported by large-scale motion datasets [64] and manual teleoperation [117]. A three-stage

skill learning paradigm, shown in Figure 3, integrates key techniques from recent work [24, 35, 96]. First, a **retargeting module** [35, 93] (Section 4.1) transfers human motions to humanoid models to generate motion animations. Next, a **motion tracking module** [24, 61, 96] (Section 4.2) is trained in simulations to execute realistic motions based on these animations, producing skill demonstrations. Finally, an **imitation learning module** [16, 62, 129] (Section 4.3) learns from these demonstrations to train humanoid agents for unseen scenarios. Our Mimicking-Bench implements this paradigm for six tasks and benchmarks advanced methods for each module, enabling comprehensive evaluation.

4.1. Humanoid Motion Retargeting

To bridge human skill references with humanoid animations, the motion retargeting module transfers motions from a human skeleton \mathcal{A} to a humanoid skeleton \mathcal{B} . To establish a correlation between \mathcal{A} and \mathcal{B} , existing retargeting approaches typically select key joints from both skeletons and manually define a joint mapping $\mathcal{M} = \{ \langle a_k, b_k \rangle \}$ [93]. These approaches then diverge into three types, each with distinct retargeting goals.

(1) **Copy-rotation:** Given a predefined joint mapping \mathcal{M} , a straightforward strategy [24] is to directly copy the joint angles from a_k to b_k . In this method, the root positions and orientations of \mathcal{B} are also copied from those of \mathcal{A} , assuming both skeletons share the same root definitions. This approach results in realistic joint orientations but does not guarantee the correctness of joint positions.

(2) **Optimization:** In contrast to copy-rotation, the optimization method [47, 81] focuses on recovering accurate joint positions while allowing for some loss in joint angle fidelity. The optimization is achieved by maximizing energy functions that incorporate constraints on joint global positions, global orientations, and joint angle ranges.

(3) **Optimization with skeleton shape alignment:** To strike a balance between joint angle fidelity and global position accuracy, recent methods [35, 36, 93] propose a two-step process. First, they adjust the bone lengths of \mathcal{A} to align with those of \mathcal{B} , and then perform optimization as described above. This adjustment alters joint positions while maintaining joint angles, while the subsequent optimization process aims to refine the joint angles.

For each human skeleton, we implement the corresponding copy-rotation and optimization algorithms, and use OmniH2O [35] to represent the optimization with skeleton shape alignment. The kinematic metric is applied to filter the obtained animations, passing only the successful ones to the next module.

4.2. Humanoid Motion Tracking

Regardless of whether the human reference motions are physical, the retargeted humanoid motion \mathcal{B} (as described in

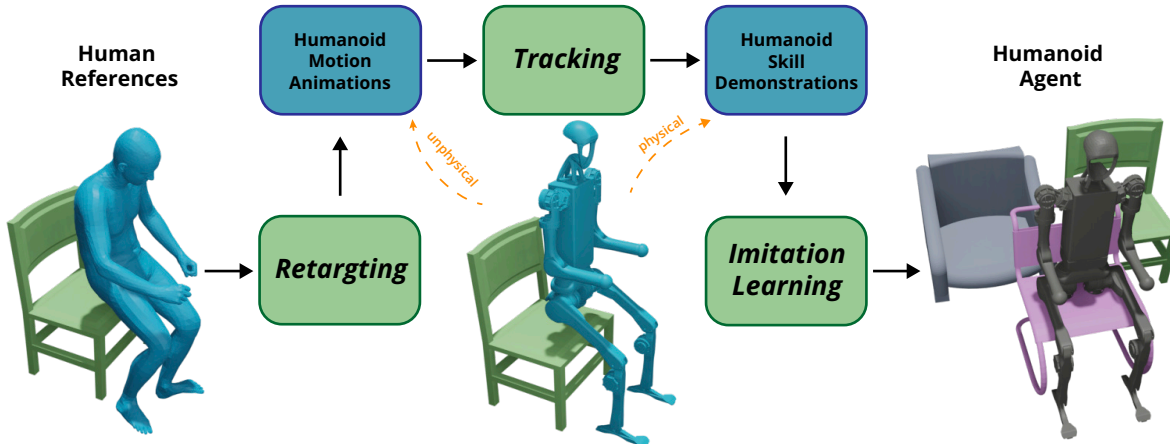


Figure 3. **Humanoid interaction skill learning paradigm.**

Section 4.1) is unphysical. To generate physical humanoid skill demonstrations and corresponding action sequences of the animation, we apply a tracking module to \mathcal{B} . For the tracking module, we benchmark HST [24] and a simplified version of PHC [61]. We briefly describe the key features and differences between these two trackers, as well as introduce the design of task-specific reward functions.

Simplified PHC [61]. PHC [61] formulates a Markov Decision Process (MDP) policy π that is trained using proximal policy optimization (PPO) [84]. At each simulation step, the policy π takes humanoid’s proprioception and goal state as inputs, and outputs the humanoid action to be performed at the next step. A proportional-derivative (PD) controller is applied to each degree of freedom (DoF) of the humanoid, with the action specifying the PD target. Reference state initialization [76] is used during training, along with early termination to stop the process when the tracking error exceeds a threshold. To simplify the training process, we use a single PHC policy, omitting the suggested composer [61] that combines multiple policies.

Improved HST [24]. Similar to PHC, HST uses PPO [84] to learn a policy generating humanoid actions based on proprioception and goal state inputs. In practice, we improve the official HST implementation [3] with redundant proprioception representations from Masked-Mimic [96], early-termination strategies inspired by Deep-Mimic [76], and motion regularization rewards for stable policy training [35, 80, 104]. The main difference between the two trackers is that the simplified PHC incorporates a higher-dimensional goal state input (primarily including state differences), whereas our improved HST includes additional reward constraints on motion energy.

Task-specific reward functions. For tasks SC, SS, LB, and LS, the primary tracking reward aims to minimize joint position and rotation angle errors between the humanoid and the reference motion \mathcal{B} . For tasks T and L, greater emphasis is placed on the motion of the hands relative to the

object (for task L, this also includes the object itself). Inspired by PhysHOI [103], we design a reward function that combines joint position, root alignment, and hand position rewards, with a higher weight assigned to the hand position. For task L, additional focus is given to the reward for object positioning and the relative relationship between the hand and the object. Details are in the appendix.

After training the motion trackers described above, we use them to track the animations from their respective training sets and obtain humanoid skill demonstrations. These demonstrations are then filtered using the kinematic metric, and only the successful ones are passed to the next module.

4.3. Humanoid Imitation Learning

As introduced in Section 2.3, the imitation learning module aims to train a generic humanoid agent using humanoid skill demonstrations, with the goal of enabling the agent to perform tasks in unseen scenarios. In our experiments, we select ACT [24] and HIT [24] as representatives of the single-stage and two-stage algorithms, respectively.

ACT [129]: ACT is a single-stage method that generates the robot’s action sequences directly from vision and proprioception inputs. It uses a CVAE-based [89] Transformer encoder-decoder structure. ACT has demonstrated superior performance on existing robot learning tasks [88] and benchmarks [15, 43].

HIT [24]: HIT is a two-stage approach that integrates a high-level, Transformer-based motion planner, which generates real-time robot animations, and a low-level motion tracker that physically mimics the animations. This method can be easily incorporated into our skill-learning paradigm by using pre-trained trackers, as described in Section 4.2.

5. Experiments

Based on the multi-stage skill learning paradigm, Mimicking-Bench supports evaluations on both integrated learning pipelines [24, 35] and modular learning algorithms [61, 129]. We conduct extensive experiments

across diverse combinations of visual input modalities (Section 3.1) and algorithm choices for different modules (Section 4), selecting the best combination as our current solution for the benchmark. This solution is then compared with existing pipelines (Section 5.1) and ablated across various modules (Sections 5.2, 5.3, 5.4), visual modalities (Section 5.5), and human reference scales (Section 5.6).

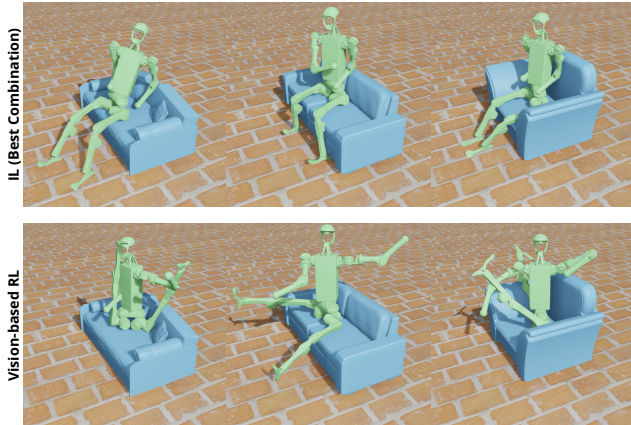


Figure 4. **Qualitative comparisons on data-driven human mimicking and data-free RL on sitting sofas.** RL struggles to get reasonable poses despite completing the task kinematically.

The best combination involves using the elevation map \mathcal{E} as the sole visual input, and employing optimization, improved HST [24], and ACT [129] for the retargeting, tracking, and imitation learning modules, respectively. We consider this solution a baseline for future research in this area.

Train-test splits: For each task, we randomly divide the objects in the dataset into training and test sets, following a 3 : 1 ratio. The training sets are used exclusively to train the modular algorithms, while the trained humanoid agents are deployed on the test sets to evaluate their generalizability.

Notations for evaluation results: In the following tables, we report both the kinematic success rate, determined by the kinematic metric (K), and the energy-averaged success rate, which is judged by K and the physical metric P using four different λ_P values, as described in Section 3.2. These two success rates are separated by a forward slash.

5.1. Skill Learning Pipelines

We compare the best combination of our methods with two existing skill learning pipelines: OmniH2O [35] and HumanPlus [24]. OmniH2O provides retargeting and tracking, to which we add our best imitation learning algorithm. HumanPlus offers an end-to-end pipeline with a novel imitation learning algorithm. Additionally, we evaluate a vision-based reinforcement learning (RL) method [84], which learns entirely through environment exploration without human references. Table 3 shows task success rates for these methods. Compared to the data-driven pipelines,

vision-based RL [84] performs significantly worse, especially in terms of physical metrics, highlighting its poor physical plausibility, as shown in Figure 4. This emphasizes the importance of learning by mimicking human references.

Existing methodologies consistently face significant challenges on tasks touching points and lifting boxes due to difficulties in stably controlling hands and manipulating dynamic objects, revealing new research opportunities.

Method	Data	SC	SS	LB	LS	T	L	Mean
PPO [84]	✗	50/25	44/20	18/9	54/26	0/0	0/0	28/13
HumanPlus [24]	✓	36/28	17/16	36/34	38/36	46/32	4/3	30/25
OmniH2O [35]	✓	79/72	69/69	48/47	47/46	0/0	0/0	41/39
Best Combination	✓	81/69	84/84	61/61	80/78	11/10	6/5	54/51

Table 3. Task success rates for different **skill learning pipelines**.

5.2. Humanoid Motion Retargeting

We evaluate the effect of combining the three motion retargeting algorithms with the best designs of other modules. Results are shown in Table 4. Studying retargeting algorithms is crucial for the success of the entire paradigm, as they directly impact the quality of humanoid motion and interaction. Among the different approaches, optimization consistently yields the best results across all settings, highlighting the importance of fine-grained positional accuracy for achieving natural and precise interactions. In tasks T and L, where hand position fidelity plays a critical role, only the optimization method can accurately capture the detailed hand movements relative to the objects, further underscoring the necessity of high precision in hand tracking.

5.3. Humanoid Motion Tracking

We ablate the humanoid motion tracking algorithm in Table 5. The results highlight that selecting the right tracking algorithm is critical for the success of the entire paradigm. Both Improved HST [24] and Simplified PHC [61] perform well on tasks SC, SS, LB, and LS. However, on tasks T and L, HST significantly outperforms PHC. The inclusion of energy rewards plays a key role, preventing excessive energy consumption and ensuring efficient, physically plausible behaviors within the maximum energy constraint. The superior performance of HST, particularly in tasks requiring precise tracking, underscores the importance of regularizers for accurate humanoid interactions.

5.4. Humanoid Imitation Learning

Table 6 compares the performance of combining two imitation learning methods with the optimal retargeting and tracking algorithms. The significant performance gap between HIT [24] and ACT [129] underscores the importance of carefully designed imitation learning algorithms within the skill learning paradigm. Compared to ACT, HIT leads to performance drops on five tasks, which may be caused by rapidly accumulating errors that push the humanoid states

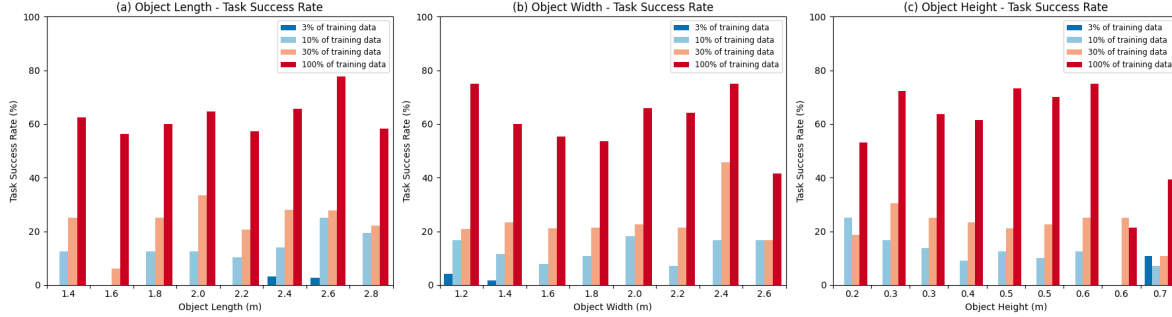


Figure 5. **LB task success rates on varying object sizes.** Object length/width refers to the size of bounding boxes and object height refers to the height of lying planes of beds.

Method	Motion Tracking Performance							Imitation Learning Performance						
	SC	SS	LB	LS	T	L	Mean	SC	SS	LB	LS	T	L	Mean
Copy-rotation	66/46	90/89	84/77	38/36	0/0	0/0	46/41	61/53	89/89	33/32	69/68	0/0	0/0	42/40
OmniH2O [35]	83/64	90/90	61/42	40/32	27/15	0/0	50/41	79/72	69/69	48/47	47/46	0/0	0/0	41/39
Optimization	92/70	90/89	88/82	55/53	58/40	25/20	68/59	81/69	84/84	61/61	80/78	11/10	6/5	54/51

Table 4. Task success rates (%) for different **motion retargeting algorithms**. Motion Tracking Performance denotes evaluation results on tracked humanoid skill demonstrations, while Imitation Learning Performance denotes evaluation results on humanoid agents.

Method	Motion Tracking Performance							Imitation Learning Performance						
	SC	SS	LB	LS	T	L	Mean	SC	SS	LB	LS	T	L	Mean
Simplified PHC [61]	87/65	92/83	63/49	80/61	8/6	0/0	55/44	44/35	69/64	14/13	71/51	0/0	0/0	33/27
Improved HST [24]	92/70	90/89	88/82	55/53	58/40	25/20	68/59	81/69	84/84	61/61	80/78	11/10	6/5	54/51

Table 5. Task success rates (%) for different **motion tracking algorithms**.

beyond the distributions of both the tracker and HIT, resulting in degraded performance.

Method	SC	SS	LB	LS	T	L	Mean
HIT [24]	36/28	17/16	36/34	38/36	46/32	4/3	30/25
ACT [35]	81/69	84/84	61/61	80/78	11/10	6/5	54/51

Table 6. Task success rates (%) for **imitation learning methods**.

5.5. Egocentric Visual Perception Modalities

With versatile choices of egocentric visual observations, Mimicking-Bench promotes studies on exploring the most effective visual modalities. We compare two common designs for visual observation in Table 7. Analyzing the results, we observe that the elevation map (\mathcal{E}) significantly outperforms the multi-view RGBD ($\mathcal{C} + \mathcal{D}$) across all tasks. One possible reason for this is the challenge of interpreting egocentric images that contain much irrelevant or noisy information, which can hinder the agent’s ability to focus on task-relevant features. In contrast, the elevation map provides a more structured and focused representation of the environment, which likely contributes to its superior performance. Based on these findings, we propose using the elevation map as the agent’s visual input and explore various technical designs under this setting.

Visual Observation	SC	SS	LB	LS	T	L	Mean
$\mathcal{C} + \mathcal{D}$	0/0	0/0	1/1	13/13	8/6	1/1	4/4
\mathcal{E}	81/69	84/84	61/61	80/78	11/10	6/5	54/51

Table 7. Task success rates (%) for different **vision modalities**.

Training Data Scale	SC	SS	LB	LS	T	L	Mean
10%	69/69	80/80	13/12	52/52	1/1	0/0	36/35
100%	81/69	84/84	61/61	80/78	11/10	6/5	54/51

Table 8. Task success rates (%) for different **training data scales**.

5.6. Scale of Human Skill Data

We compare the results of the best algorithm combination under different scales of human references. The comparison between 10% and 100% training data in Table 8 highlights the impact of data scale on performance. As expected, a larger training dataset leads to improved task success across most metrics. Specifically, increasing the data scale from 10% to 100% significantly boosts performance in tasks such as SC, SS, LB, and LS. For LB task, we expand the data scale comparison among 3%, 10%, 30% and 100%. Results in Fig. 5 show a significant performance improvement as the data scale increases, particularly for objects of extreme sizes. This demonstrates that large-scale data is crucial for training robust models, confirming the usefulness of our large-scale dataset for improving generalizability and performance across various tasks.

6. Limitation and Conclusion

We introduce Mimicking-Bench, the first comprehensive benchmark designed to support generalizable humanoid-scene interaction skill learning through the mimicking of human references. It encompasses six diverse tasks and an integrated human reference dataset, featuring 11K object shapes and 23K human-scene interaction motions. To advance research on various technical challenges, we present

a generic humanoid interaction skill learning paradigm comprising three key modules, alongside pipeline-wise and modular method comparisons. Extensive experiments demonstrate the effectiveness of learning from human imitation, highlight the importance of selecting appropriate algorithms for each module, and identify new challenges and research opportunities for existing methodologies.

Limitation. Our robot model does not include dexterous hands, as our focus is primarily on torso-level interaction. Future work could explore incorporating hands, which would enable the study of fine-grained manipulation skills.

References

- [1] Act. <https://github.com/tonyzhaozh/act>, 2024. 15, 16
- [2] Franka. <https://franka.de/>, 2024. 2
- [3] Humanplus. <https://github.com/MarkFzp/humanplus>, 2024. 6, 15
- [4] Josh Achiam, Steven Adler, Sandhini Agarwal, Lama Ahmad, Ilge Akkaya, Florencia Leoni Aleman, Diogo Almeida, Janko Altenschmidt, Sam Altman, Shyamal Anadkat, et al. Gpt-4 technical report. *arXiv preprint arXiv:2303.08774*, 2023. 3
- [5] Firas Al-Hafez, Guoping Zhao, Jan Peters, and Davide Tateo. Locomujoco: A comprehensive imitation learning benchmark for locomotion. *arXiv preprint arXiv:2311.02496*, 2023. 2, 4
- [6] Joao Pedro Araujo, Jiaman Li, Karthik Vetrivel, Rishi Agarwal, Jiajun Wu, Deepak Gopinath, Alexander William Clegg, and Karen Liu. Circle: Capture in rich contextual environments. In *Proceedings of the IEEE/CVF Conference on Computer Vision and Pattern Recognition*, pages 21211–21221, 2023. 3
- [7] Bharat Lal Bhatnagar, Xianghui Xie, Ilya A Petrov, Cristian Sminchisescu, Christian Theobalt, and Gerard Pons-Moll. Behave: Dataset and method for tracking human object interactions. In *Proceedings of the IEEE/CVF Conference on Computer Vision and Pattern Recognition*, pages 15935–15946, 2022. 3
- [8] G Brockman. Openai gym. *arXiv preprint arXiv:1606.01540*, 2016. 2, 4
- [9] Angel X Chang, Thomas Funkhouser, Leonidas Guibas, Pat Hanrahan, Qixing Huang, Zimo Li, Silvio Savarese, Manolis Savva, Shuran Song, Hao Su, et al. Shapenet: An information-rich 3d model repository. *arXiv preprint arXiv:1512.03012*, 2015. 5
- [10] Yu-Wei Chao, Jimei Yang, Weifeng Chen, and Jia Deng. Learning to sit: Synthesizing human-chair interactions via hierarchical control. In *Proceedings of the AAAI Conference on Artificial Intelligence*, pages 5887–5895, 2021. 15
- [11] Zixuan Chen, Xialin He, Yen-Jen Wang, Qiayuan Liao, Yanjie Ze, Zhongyu Li, S Shankar Sastry, Jiajun Wu, Koushil Sreenath, Saurabh Gupta, et al. Learning smooth humanoid locomotion through lipschitz-constrained policies. *arXiv preprint arXiv:2410.11825*, 2024. 1
- [12] Xuxin Cheng, Yandong Ji, Junming Chen, Ruihan Yang, Ge Yang, and Xiaolong Wang. Expressive whole-body control for humanoid robots. *arXiv preprint arXiv:2402.16796*, 2024. 15
- [13] Xuxin Cheng, Jialong Li, Shiqi Yang, Ge Yang, and Xiaolong Wang. Open-television: Teleoperation with immersive active visual feedback. *arXiv preprint arXiv:2407.01512*, 2024. 15
- [14] Nuttapon Chentanez, Matthias Müller, Miles Macklin, Viktor Makoviychuk, and Stefan Jeschke. Physics-based motion capture imitation with deep reinforcement learning. In *Proceedings of the 11th ACM SIGGRAPH Conference on Motion, Interaction and Games*, pages 1–10, 2018. 15
- [15] Nikita Chernyadev, Nicholas Backshall, Xiao Ma, Yunfan Lu, Younggyo Seo, and Stephen James. Bigym: A demodriven mobile bi-manual manipulation benchmark. *arXiv preprint arXiv:2407.07788*, 2024. 2, 3, 4, 6
- [16] Cheng Chi, Siyuan Feng, Yilun Du, Zhenjia Xu, Eric Cousineau, Benjamin Burchfiel, and Shuran Song. Diffusion policy: Visuomotor policy learning via action diffusion. *arXiv preprint arXiv:2303.04137*, 2023. 2, 5, 15, 16
- [17] Jieming Cui, Tengyu Liu, Nian Liu, Yaodong Yang, Yixin Zhu, and Siyuan Huang. Anyskill: Learning open-vocabulary physical skill for interactive agents. In *Proceedings of the IEEE/CVF Conference on Computer Vision and Pattern Recognition*, pages 852–862, 2024. 3
- [18] Jeremy Dao, Helei Duan, and Alan Fern. Sim-to-real learning for humanoid box loco-manipulation. In *2024 IEEE International Conference on Robotics and Automation (ICRA)*, pages 16930–16936. IEEE, 2024. 2
- [19] Christian Diller and Angela Dai. Cg-hoi: Contact-guided 3d human-object interaction generation. *arXiv preprint arXiv:2311.16097*, 2023. 3
- [20] Zhiyang Dou, Xuelin Chen, Qingnan Fan, Taku Komura, and Wenping Wang. C-ase: Learning conditional adversarial skill embeddings for physics-based characters. In *SIGGRAPH Asia 2023 Conference Papers*, pages 1–11, 2023. 3
- [21] Pranay Dugar, Aayam Shrestha, Fangzhou Yu, Bart van Marum, and Alan Fern. Learning multi-modal whole-body control for real-world humanoid robots. *arXiv preprint arXiv:2408.07295*, 2024. 15
- [22] Boston Dynamics. Atlas. <https://bostondynamics.com/atlas>, 2024. 1
- [23] Siyuan Feng, Eric Whitman, X Xinjilefu, and Christopher G Atkeson. Optimization based full body control for the atlas robot. In *2014 IEEE-RAS International Conference on Humanoid Robots*, pages 120–127. IEEE, 2014. 1, 2
- [24] Zipeng Fu, Qingqing Zhao, Qi Wu, Gordon Wetzstein, and Chelsea Finn. Humanplus: Humanoid shadowing and imitation from humans. *arXiv preprint arXiv:2406.10454*, 2024. 2, 3, 4, 5, 6, 7, 8, 15, 16, 19, 20
- [25] Levi Fussell, Kevin Bergamin, and Daniel Holden. Super-track: Motion tracking for physically simulated characters using supervised learning. *ACM Transactions on Graphics (TOG)*, 40(6):1–13, 2021. 15

- [26] Jiawei Gao, Ziqin Wang, Zeqi Xiao, Jingbo Wang, Tai Wang, Jinkun Cao, Xiaolin Hu, Si Liu, Jifeng Dai, and Jiangmiao Pang. Coohei: Learning cooperative human-object interaction with manipulated object dynamics. *arXiv preprint arXiv:2406.14558*, 2024. **3**
- [27] Ian Goodfellow, Jean Pouget-Abadie, Mehdi Mirza, Bing Xu, David Warde-Farley, Sherjil Ozair, Aaron Courville, and Yoshua Bengio. Generative adversarial networks. *Communications of the ACM*, 63(11):139–144, 2020. **3**
- [28] Jiayuan Gu, Fanbo Xiang, Xuanlin Li, Zhan Ling, Xiqiang Liu, Tongzhou Mu, Yihe Tang, Stone Tao, Xinyue Wei, Yunchao Yao, et al. Maniskill2: A unified benchmark for generalizable manipulation skills. *arXiv preprint arXiv:2302.04659*, 2023. **2, 4**
- [29] Xinyang Gu, Yen-Jen Wang, and Jianyu Chen. Humanoid-gym: Reinforcement learning for humanoid robot with zero-shot sim2real transfer. *arXiv preprint arXiv:2404.05695*, 2024. **1**
- [30] Nicklas Hansen, Hao Su, and Xiaolong Wang. Td-mpc2: Scalable, robust world models for continuous control. *arXiv preprint arXiv:2310.16828*, 2023. **2**
- [31] Nicklas Hansen, Jyothir SV, Vlad Sobal, Yann LeCun, Xiaolong Wang, and Hao Su. Hierarchical world models as visual whole-body humanoid controllers. *arXiv preprint arXiv:2405.18418*, 2024. **15**
- [32] Mohamed Hassan, Vasileios Choutas, Dimitrios Tzionas, and Michael J Black. Resolving 3d human pose ambiguities with 3d scene constraints. In *Proceedings of the IEEE/CVF international conference on computer vision*, pages 2282–2292, 2019. **3**
- [33] Mohamed Hassan, Duygu Ceylan, Ruben Villegas, Jun Saito, Jimei Yang, Yi Zhou, and Michael J Black. Stochastic scene-aware motion prediction. In *Proceedings of the IEEE/CVF International Conference on Computer Vision*, pages 11374–11384, 2021. **2, 3**
- [34] Mohamed Hassan, Yunrong Guo, Tingwu Wang, Michael Black, Sanja Fidler, and Xue Bin Peng. Synthesizing physical character-scene interactions. In *ACM SIGGRAPH 2023 Conference Proceedings*, pages 1–9, 2023. **3, 5**
- [35] Tairan He, Zhengyi Luo, Xialin He, Wenli Xiao, Chong Zhang, Weinan Zhang, Kris Kitani, Changliu Liu, and Guanya Shi. Omnih2o: Universal and dexterous human-to-humanoid whole-body teleoperation and learning. *arXiv preprint arXiv:2406.08858*, 2024. **2, 3, 4, 5, 6, 7, 8, 15, 18**
- [36] Tairan He, Zhengyi Luo, Wenli Xiao, Chong Zhang, Kris Kitani, Changliu Liu, and Guanya Shi. Learning human-to-humanoid real-time whole-body teleoperation. *arXiv preprint arXiv:2403.04436*, 2024. **5, 15**
- [37] Tairan He, Wenli Xiao, Toru Lin, Zhengyi Luo, Zhenjia Xu, Zhenyu Jiang, Jan Kautz, Changliu Liu, Guanya Shi, Xiaolong Wang, et al. Hover: Versatile neural whole-body controller for humanoid robots. *arXiv preprint arXiv:2410.21229*, 2024. **2**
- [38] Minh Heo, Youngwoon Lee, Doohyun Lee, and Joseph J Lim. Furniturebench: Reproducible real-world benchmark for long-horizon complex manipulation. *arXiv preprint arXiv:2305.12821*, 2023. **2, 4**
- [39] Yinghao Huang, Omid Taheri, Michael J Black, and Dimitrios Tzionas. Intercap: Joint markerless 3d tracking of humans and objects in interaction. In *DAGM German Conference on Pattern Recognition*, pages 281–299. Springer, 2022. **3**
- [40] Catalin Ionescu, Dragos Papava, Vlad Olaru, and Cristian Sminchisescu. Human3.6m: Large scale datasets and predictive methods for 3d human sensing in natural environments. *IEEE transactions on pattern analysis and machine intelligence*, 36(7):1325–1339, 2013. **15**
- [41] Stephen James, Zicong Ma, David Rovick Arrojo, and Andrew J Davison. Rlbench: The robot learning benchmark & learning environment. *IEEE Robotics and Automation Letters*, 5(2):3019–3026, 2020. **2, 4**
- [42] Fabian Jenelten, Junzhe He, Farbod Farshidian, and Marco Hutter. Dtc: Deep tracking control. *Science Robotics*, 9(86):eadh5401, 2024. **3**
- [43] Xiaogang Jia, Denis Blessing, Xinkai Jiang, Moritz Reuss, Atalay Donat, Rudolf Lioutikov, and Gerhard Neumann. Towards diverse behaviors: A benchmark for imitation learning with human demonstrations. *arXiv preprint arXiv:2402.14606*, 2024. **2, 4, 6**
- [44] Nan Jiang, Tengyu Liu, Zhexiong Cao, Jieming Cui, Zhiyuan Zhang, Yixin Chen, He Wang, Yixin Zhu, and Siyuan Huang. Full-body articulated human-object interaction. In *Proceedings of the IEEE/CVF International Conference on Computer Vision*, pages 9365–9376, 2023. **2, 3**
- [45] Nan Jiang, Zhiyuan Zhang, Hongjie Li, Xiaoxuan Ma, Zan Wang, Yixin Chen, Tengyu Liu, Yixin Zhu, and Siyuan Huang. Scaling up dynamic human-scene interaction modeling. *arXiv preprint arXiv:2403.08629*, 2024. **3**
- [46] Nan Jiang, Zhiyuan Zhang, Hongjie Li, Xiaoxuan Ma, Zan Wang, Yixin Chen, Tengyu Liu, Yixin Zhu, and Siyuan Huang. Scaling up dynamic human-scene interaction modeling. In *Proceedings of the IEEE/CVF Conference on Computer Vision and Pattern Recognition*, pages 1737–1747, 2024. **4**
- [47] Zhenyu Jiang, Yuqi Xie, Jinhan Li, Ye Yuan, Yifeng Zhu, and Yuke Zhu. Harmon: Whole-body motion generation of humanoid robots from language descriptions. *arXiv preprint arXiv:2410.12773*, 2024. **5**
- [48] Zhenyu Jiang, Yuqi Xie, Kevin Lin, Zhenjia Xu, Weikang Wan, Ajay Mandlekar, Linxi Fan, and Yuke Zhu. Dexmimicgen: Automated data generation for bimanual dexterous manipulation via imitation learning. *arXiv preprint arXiv:2410.24185*, 2024. **15**
- [49] Jordan Juravsky, Yunrong Guo, Sanja Fidler, and Xue Bin Peng. Padl: Language-directed physics-based character control. In *SIGGRAPH Asia 2022 Conference Papers*, pages 1–9, 2022. **3**
- [50] Nazmul Karim, Mamshad Nayeem Rizve, Nazanin Rahnavard, Ajmal Mian, and Mubarak Shah. Unicon: Combating label noise through uniform selection and contrastive learning. In *Proceedings of the IEEE/CVF conference on computer vision and pattern recognition*, pages 9676–9686, 2022. **15**

- [51] Kunio Kojima, Tatsuhi Karasawa, Toyotaka Kozuki, Eisoku Kuroiwa, Sou Yukizaki, Satoshi Iwaishi, Tatsuya Ishikawa, Ryo Koyama, Shintaro Noda, Fumihito Sugai, et al. Development of life-sized high-power humanoid robot jaxon for real-world use. In *2015 IEEE-RAS 15th International Conference on Humanoid Robots (Humanoids)*, pages 838–843. IEEE, 2015. [2](#)
- [52] Nilesh Kulkarni, Davis Rempe, Kyle Genova, Abhijit Kundu, Justin Johnson, David Fouhey, and Leonidas Guibas. Nifty: Neural object interaction fields for guided human motion synthesis. *arXiv preprint arXiv:2307.07511*, 2023. [3](#)
- [53] Vikash Kumar, Zhe Xu, and Emanuel Todorov. Fast, strong and compliant pneumatic actuation for dexterous tendon-driven hands. In *2013 IEEE international conference on robotics and automation*, pages 1512–1519. IEEE, 2013. [2](#)
- [54] Jiaman Li, Alexander Clegg, Roozbeh Mottaghi, Jiajun Wu, Xavier Puig, and C Karen Liu. Controllable human-object interaction synthesis. *arXiv preprint arXiv:2312.03913*, 2023. [3](#)
- [55] Jiaman Li, Jiajun Wu, and C Karen Liu. Object motion guided human motion synthesis. *ACM Transactions on Graphics (TOG)*, 42(6):1–11, 2023. [3](#)
- [56] Jinhan Li, Yifeng Zhu, Yuqi Xie, Zhenyu Jiang, Mingyo Seo, Georgios Pavlakos, and Yuke Zhu. Okami: Teaching humanoid robots manipulation skills through single video imitation. *arXiv preprint arXiv:2410.11792*, 2024. [2](#), [15](#)
- [57] Qiayuan Liao, Bike Zhang, Xuanyu Huang, Xiaoyu Huang, Zhongyu Li, and Koushil Sreenath. Berkeley humanoid: A research platform for learning-based control. *arXiv preprint arXiv:2407.21781*, 2024. [1](#)
- [58] Fukang Liu, Zhaoyuan Gu, Yilin Cai, Ziyi Zhou, Shijie Zhao, Hyunyoung Jung, Sehoon Ha, Yue Chen, Danfei Xu, and Ye Zhao. Opt2skill: Imitating dynamically-feasible whole-body trajectories for versatile humanoid loco-manipulation. *arXiv preprint arXiv:2409.20514*, 2024. [2](#)
- [59] Yunze Liu, Changxi Chen, and Li Yi. Interactive humanoid: Online full-body motion reaction synthesis with social affordance canonicalization and forecasting. *arXiv preprint arXiv:2312.08983*, 2023. [3](#)
- [60] Zhengyi Luo, Ryo Hachiuma, Ye Yuan, and Kris Kitani. Dynamics-regulated kinematic policy for egocentric pose estimation. *Advances in Neural Information Processing Systems*, 34:25019–25032, 2021. [15](#)
- [61] Zhengyi Luo, Jinkun Cao, Kris Kitani, Weipeng Xu, et al. Perpetual humanoid control for real-time simulated avatars. In *Proceedings of the IEEE/CVF International Conference on Computer Vision*, pages 10895–10904, 2023. [5](#), [6](#), [7](#), [8](#), [15](#), [19](#)
- [62] Zhengyi Luo, Jinkun Cao, Josh Merel, Alexander Winkler, Jing Huang, Kris Kitani, and Weipeng Xu. Universal humanoid motion representations for physics-based control. *arXiv preprint arXiv:2310.04582*, 2023. [3](#), [5](#), [15](#)
- [63] Zhengyi Luo, Jiashun Wang, Kangni Liu, Haotian Zhang, Chen Tessler, Jingbo Wang, Ye Yuan, Jinkun Cao, Zihui Lin, Fengyi Wang, et al. Smpolympics: Sports environments for physically simulated humanoids. *arXiv preprint arXiv:2407.00187*, 2024. [3](#)
- [64] Naureen Mahmood, Nima Ghorbani, Nikolaus F Troje, Gerard Pons-Moll, and Michael J Black. Amass: Archive of motion capture as surface shapes. In *Proceedings of the IEEE/CVF international conference on computer vision*, pages 5442–5451, 2019. [5](#), [15](#)
- [65] Viktor Makovychuk, Lukasz Wawrzyniak, Yunrong Guo, Michelle Lu, Kier Storey, Miles Macklin, David Hoeller, Nikita Rudin, Arthur Allshire, Ankur Handa, et al. Isaac gym: High performance gpu-based physics simulation for robot learning. *arXiv preprint arXiv:2108.10470*, 2021. [3](#)
- [66] Daniel Marew, Nisal Perera, Shangqun Yu, Sarah Roelker, and Donghyun Kim. A biomechanics-inspired approach to soccer kicking for humanoid robots. *arXiv preprint arXiv:2407.14612*, 2024. [15](#)
- [67] Raphael Memmesheimer, Ivanna Kramer, Viktor Seib, and Dietrich Paulus. Simitate: A hybrid imitation learning benchmark. In *2019 IEEE/RSJ International Conference on Intelligent Robots and Systems (IROS)*, pages 5243–5249. IEEE, 2019. [2](#)
- [68] Xiang Meng, Zhangguo Yu, Xuechao Chen, Zelin Huang, Fei Meng, and Qiang Huang. Online adaptive motion generation for humanoid locomotion on non-flat terrain via template behavior extension. *IEEE Transactions on Automation Science and Engineering*, 2023. [1](#)
- [69] Josh Merel, Saran Tunyasuvunakool, Arun Ahuja, Yuval Tassa, Leonard Hasenclever, Vu Pham, Tom Erez, Greg Wayne, and Nicolas Heess. Catch & carry: reusable neural controllers for vision-guided whole-body tasks. *ACM Transactions on Graphics (TOG)*, 39(4):39–1, 2020. [2](#), [3](#), [15](#)
- [70] Takahiro Miki, Lorenz Wellhausen, Ruben Grandia, Fabian Jenelten, Timon Homberger, and Marco Hutter. Elevation mapping for locomotion and navigation using gpu. In *2022 IEEE/RSJ International Conference on Intelligent Robots and Systems (IROS)*, pages 2273–2280. IEEE, 2022. [3](#), [17](#)
- [71] Kaichun Mo, Shilin Zhu, Angel X. Chang, Li Yi, Subarna Tripathi, Leonidas J. Guibas, and Hao Su. PartNet: A large-scale benchmark for fine-grained and hierarchical part-level 3D object understanding. In *The IEEE Conference on Computer Vision and Pattern Recognition (CVPR)*, 2019. [5](#)
- [72] Tongzhou Mu, Zhan Ling, Fanbo Xiang, Derek Yang, Xuanlin Li, Stone Tao, Zhiao Huang, Zhiwei Jia, and Hao Su. Maniskill: Generalizable manipulation skill benchmark with large-scale demonstrations. *arXiv preprint arXiv:2107.14483*, 2021. [2](#), [4](#)
- [73] Liang Pan, Jingbo Wang, Buzhen Huang, Junyu Zhang, Haofan Wang, Xu Tang, and Yangang Wang. Synthesizing physically plausible human motions in 3d scenes. In *2024 International Conference on 3D Vision (3DV)*, pages 1498–1507. IEEE, 2024. [3](#)
- [74] Georgios Pavlakos, Vasileios Choutas, Nima Ghorbani, Timo Bolkart, Ahmed AA Osman, Dimitrios Tzionas, and Michael J Black. Expressive body capture: 3d hands, face, and body from a single image. In *Proceedings of the IEEE/CVF conference on computer vision and pattern recognition*, pages 10975–10985, 2019. [18](#)

- [75] Xiaogang Peng, Yiming Xie, Zizhao Wu, Varun Jampani, Deqing Sun, and Huaizu Jiang. Hoi-diff: Text-driven synthesis of 3d human-object interactions using diffusion models. *arXiv preprint arXiv:2312.06553*, 2023. 3
- [76] Xue Bin Peng, Pieter Abbeel, Sergey Levine, and Michiel Van de Panne. Deepmimic: Example-guided deep reinforcement learning of physics-based character skills. *ACM Transactions On Graphics (TOG)*, 37(4):1–14, 2018. 6, 15, 19
- [77] Xue Bin Peng, Ze Ma, Pieter Abbeel, Sergey Levine, and Angjoo Kanazawa. Amp: Adversarial motion priors for stylized physics-based character control. *ACM Transactions on Graphics (ToG)*, 40(4):1–20, 2021. 3, 5
- [78] Xue Bin Peng, Yunrong Guo, Lina Halper, Sergey Levine, and Sanja Fidler. Ase: Large-scale reusable adversarial skill embeddings for physically simulated characters. *ACM Transactions On Graphics (TOG)*, 41(4):1–17, 2022. 3
- [79] Matthias Plappert, Marcin Andrychowicz, Alex Ray, Bob McGrew, Bowen Baker, Glenn Powell, Jonas Schneider, Josh Tobin, Maciek Chociej, Peter Welinder, et al. Multi-goal reinforcement learning: Challenging robotics environments and request for research. *arXiv preprint arXiv:1802.09464*, 2018. 4
- [80] Tiffany Portela, Gabriel B Margolis, Yandong Ji, and Pulkit Agrawal. Learning force control for legged manipulation. *arXiv preprint arXiv:2405.01402*, 2024. 6
- [81] Ilija Radosavovic, Bike Zhang, Baifeng Shi, Jathushan Rajasegaran, Sarthak Kamat, Trevor Darrell, Koushil Sreenath, and Jitendra Malik. Humanoid locomotion as next token prediction. *arXiv preprint arXiv:2402.19469*, 2024. 1, 2, 3, 5, 15
- [82] Davis Rempe, Zhengyi Luo, Xue Bin Peng, Ye Yuan, Kris Kitani, Karsten Kreis, Sanja Fidler, and Or Litany. Trace and pace: Controllable pedestrian animation via guided trajectory diffusion. In *Proceedings of the IEEE/CVF Conference on Computer Vision and Pattern Recognition*, pages 13756–13766, 2023. 3
- [83] Jiawei Ren, Cunjun Yu, Siwei Chen, Xiao Ma, Liang Pan, and Ziwei Liu. Diffmimic: Efficient motion mimicking with differentiable physics. *arXiv preprint arXiv:2304.03274*, 2023. 15
- [84] John Schulman, Filip Wolski, Prafulla Dhariwal, Alec Radford, and Oleg Klimov. Proximal policy optimization algorithms. *arXiv preprint arXiv:1707.06347*, 2017. 2, 6, 7, 19
- [85] Mingyo Seo, Steve Han, Kyutae Sim, Seung Hyeon Bang, Carlos Gonzalez, Luis Sentis, and Yuke Zhu. Deep imitation learning for humanoid loco-manipulation through human teleoperation. In *2023 IEEE-RAS 22nd International Conference on Humanoid Robots (Humanoids)*, pages 1–8. IEEE, 2023. 1, 15
- [86] Agon Serifi, Ruben Grandia, Espen Knoop, Markus Gross, and Moritz Bächer. Vmp: Versatile motion priors for robustly tracking motion on physical characters. In *Proceedings of the ACM SIGGRAPH/Eurographics Symposium on Computer Animation*, pages 1–11, 2024. 15
- [87] Carmelo Sferrazza, Dun-Ming Huang, Xingyu Lin, Youngwoon Lee, and Pieter Abbeel. Humanoidbench: Simulated humanoid benchmark for whole-body locomotion and manipulation. *arXiv preprint arXiv:2403.10506*, 2024. 2, 4
- [88] Lucy Xiaoyang Shi, Archit Sharma, Tony Z Zhao, and Chelsea Finn. Waypoint-based imitation learning for robotic manipulation. *arXiv preprint arXiv:2307.14326*, 2023. 6
- [89] Kihyuk Sohn, Honglak Lee, and Xinchen Yan. Learning structured output representation using deep conditional generative models. *Advances in neural information processing systems*, 28, 2015. 6
- [90] Sebastian Starke, He Zhang, Taku Komura, and Jun Saito. Neural state machine for character-scene interactions. *ACM Trans. Graph.*, 38(6):209–1, 2019. 3
- [91] Sebastian Starke, He Zhang, Taku Komura, and Jun Saito. Neural state machine for character-scene interactions. *ACM Transactions on Graphics*, 38(6):178, 2019. 4
- [92] Zhuo Su, Lan Xu, Dawei Zhong, Zhong Li, Fan Deng, Shuxue Quan, and Lu Fang. Robustfusion: Robust volumetric performance reconstruction under human-object interactions from monocular rgbd stream. *IEEE Transactions on Pattern Analysis and Machine Intelligence*, 45(5):6196–6213, 2022. 3
- [93] Annan Tang, Takuma Hiraoka, Naoki Hiraoka, Fan Shi, Kento Kawaharazuka, Kunio Kojima, Kei Okada, and Masayuki Inaba. Humanmimic: Learning natural locomotion and transitions for humanoid robot via wasserstein adversarial imitation. In *2024 IEEE International Conference on Robotics and Automation (ICRA)*, pages 13107–13114. IEEE, 2024. 1, 2, 3, 5, 18
- [94] Yuval Tassa, Yotam Doron, Alistair Muldal, Tom Erez, Yazhe Li, Diego de Las Casas, David Budden, Abbas Abdolmaleki, Josh Merel, Andrew Lefrancq, et al. Deepmind control suite. *arXiv preprint arXiv:1801.00690*, 2018. 2, 4
- [95] Chen Tessler, Yoni Kasten, Yunrong Guo, Shie Mannor, Gal Chechik, and Xue Bin Peng. Calm: Conditional adversarial latent models for directable virtual characters. In *ACM SIGGRAPH 2023 Conference Proceedings*, pages 1–9, 2023. 3
- [96] Chen Tessler, Yunrong Guo, Ofir Nabati, Gal Chechik, and Xue Bin Peng. Maskedmimic: Unified physics-based character control through masked motion inpainting. *arXiv preprint arXiv:2409.14393*, 2024. 2, 3, 5, 6, 15
- [97] Guy Tevet, Sigal Raab, Setareh Cohan, Daniele Reda, Zhengyi Luo, Xue Bin Peng, Amit H Bermano, and Michiel van de Panne. Cload: Closing the loop between simulation and diffusion for multi-task character control. *arXiv preprint arXiv:2410.03441*, 2024. 15
- [98] Takara E Truong, Michael Pisen, Zhaoming Xie, and C Karen Liu. Pdp: Physics-based character animation via diffusion policy. *arXiv preprint arXiv:2406.00960*, 2024. 15
- [99] Unitree. Unitree’s first universal humanoid robot. <https://www.unitree.com/h1>, 2018. 1, 2, 3
- [100] Unitree. Unitree rl gym. https://github.com/unitreerobotics/unitree_rl_gym, 2024. 3
- [101] Nolan Wagnier, Andrey Kolobov, Felipe Vieira Frujeri, Ricky Loynd, Ching-An Cheng, and Matthew Hausknecht.

- Mocapact: A multi-task dataset for simulated humanoid control. *Advances in Neural Information Processing Systems*, 35:35418–35431, 2022. 15
- [102] Jingbo Wang, Zhengyi Luo, Ye Yuan, Yixuan Li, and Bo Dai. Pacer+: On-demand pedestrian animation controller in driving scenarios. In *Proceedings of the IEEE/CVF Conference on Computer Vision and Pattern Recognition*, pages 718–728, 2024. 3
- [103] Yinhuai Wang, Jing Lin, Ailing Zeng, Zhengyi Luo, Jian Zhang, and Lei Zhang. Physshoi: Physics-based imitation of dynamic human-object interaction. *arXiv preprint arXiv:2312.04393*, 2023. 6, 15
- [104] Yinhuai Wang, Qihan Zhao, Runyi Yu, Ailing Zeng, Jing Lin, Zhengyi Luo, Hok Wai Tsui, Jiwen Yu, Xiu Li, Qifeng Chen, et al. Skillmimic: Learning reusable basketball skills from demonstrations. *arXiv preprint arXiv:2408.15270*, 2024. 3, 6, 15
- [105] Zan Wang, Yixin Chen, Tengyu Liu, Yixin Zhu, Wei Liang, and Siyuan Huang. Humanise: Language-conditioned human motion generation in 3d scenes. *Advances in Neural Information Processing Systems*, 35:14959–14971, 2022. 3
- [106] Noah Wiederhold, Ava Megyeri, DiMaggio Paris, Sean Banerjee, and Natasha Banerjee. Hoh: Markerless multimodal human-object-human handover dataset with large object count. *Advances in Neural Information Processing Systems*, 36, 2024. 3
- [107] Jungdam Won, Deepak Gopinath, and Jessica Hodgins. A scalable approach to control diverse behaviors for physically simulated characters. *ACM Transactions on Graphics (TOG)*, 39(4):33–1, 2020. 15
- [108] Zeqi Xiao, Tai Wang, Jingbo Wang, Jinkun Cao, Wenwei Zhang, Bo Dai, Dahua Lin, and Jiangmiao Pang. Unified human-scene interaction via prompted chain-of-contacts. *arXiv preprint arXiv:2309.07918*, 2023. 2, 3, 4, 5, 18
- [109] Xianghui Xie, Bharat Lal Bhatnagar, and Gerard Pons-Moll. Chore: Contact, human and object reconstruction from a single rgb image. In *European Conference on Computer Vision*, pages 125–145. Springer, 2022. 3
- [110] Xianghui Xie, Bharat Lal Bhatnagar, and Gerard Pons-Moll. Visibility aware human-object interaction tracking from single rgb camera. In *Proceedings of the IEEE/CVF Conference on Computer Vision and Pattern Recognition*, pages 4757–4768, 2023.
- [111] Xianghui Xie, Jan Eric Lenssen, and Gerard Pons-Moll. Intertrack: Tracking human object interaction without object templates. *arXiv preprint arXiv:2408.13953*, 2024. 3
- [112] Zhaoming Xie, Jonathan Tseng, Sebastian Starke, Michiel van de Panne, and C Karen Liu. Hierarchical planning and control for box loco-manipulation. *Proceedings of the ACM on Computer Graphics and Interactive Techniques*, 6(3):1–18, 2023. 15
- [113] Sirui Xu, Zhengyuan Li, Yu-Xiong Wang, and Liang-Yan Gui. Interdiff: Generating 3d human-object interactions with physics-informed diffusion. In *Proceedings of the IEEE/CVF International Conference on Computer Vision*, pages 14928–14940, 2023. 3
- [114] Sirui Xu, Ziyin Wang, Yu-Xiong Wang, and Liang-Yan Gui. Interdreamer: Zero-shot text to 3d dynamic human-object interaction. *arXiv preprint arXiv:2403.19652*, 2024. 3
- [115] Heyuan Yao, Zhenhua Song, Yuyang Zhou, Tenglong Ao, Baoquan Chen, and Libin Liu. Moconvq: Unified physics-based motion control via scalable discrete representations. *ACM Transactions on Graphics (TOG)*, 43(4):1–21, 2024. 15
- [116] Tianhe Yu, Deirdre Quillen, Zhanpeng He, Ryan Julian, Karol Hausman, Chelsea Finn, and Sergey Levine. Meta-world: A benchmark and evaluation for multi-task and meta reinforcement learning. In *Conference on robot learning*, pages 1094–1100. PMLR, 2020. 2, 4
- [117] Yanjie Ze, Zixuan Chen, Wenhao Wang, Tianyi Chen, Xialin He, Ying Yuan, Xue Bin Peng, and Jiajun Wu. Generalizable humanoid manipulation with improved 3d diffusion policies. *arXiv preprint arXiv:2410.10803*, 2024. 2, 5, 15
- [118] Chengwen Zhang, Yun Liu, Ruofan Xing, Bingda Tang, and Li Yi. Core4d: A 4d human-object-human interaction dataset for collaborative object rearrangement. *arXiv preprint arXiv:2406.19353*, 2024. 2, 3, 5, 18
- [119] Chong Zhang, Wenli Xiao, Tairan He, and Guanya Shi. Wococo: Learning whole-body humanoid control with sequential contacts. *arXiv preprint arXiv:2406.06005*, 2024. 2, 4
- [120] Juze Zhang, Haimin Luo, Hongdi Yang, Xinru Xu, Qianyang Wu, Ye Shi, Jingyi Yu, Lan Xu, and Jingya Wang. Neurdome: A neural modeling pipeline on multi-view human-object interactions. In *Proceedings of the IEEE/CVF Conference on Computer Vision and Pattern Recognition*, pages 8834–8845, 2023. 3
- [121] Siwei Zhang, Qianli Ma, Yan Zhang, Zhiyin Qian, Taemin Kwon, Marc Pollefeys, Federica Bogo, and Siyu Tang. Ego-body: Human body shape and motion of interacting people from head-mounted devices. In *European Conference on Computer Vision*, pages 180–200. Springer, 2022. 3
- [122] Wanyue Zhang, Rishabh Dabral, Thomas Leimkühler, Vladislav Golyanik, Marc Habermann, and Christian Theobalt. Roam: Robust and object-aware motion generation using neural pose descriptors. In *2024 International Conference on 3D Vision (3DV)*, pages 1392–1402. IEEE, 2024. 2, 3, 4, 5, 18
- [123] Xiaohan Zhang, Bharat Lal Bhatnagar, Sebastian Starke, Vladimir Guzov, and Gerard Pons-Moll. Couch: Towards controllable human-chair interactions. In *European Conference on Computer Vision*, pages 518–535. Springer, 2022. 3
- [124] Xiaohan Zhang, Bharat Lal Bhatnagar, Sebastian Starke, Vladimir Guzov, and Gerard Pons-Moll. Couch: Towards controllable human-chair interactions. In *European Conference on Computer Vision*, pages 518–535. Springer, 2022. 2, 4
- [125] Xiaohan Zhang, Bharat Lal Bhatnagar, Sebastian Starke, Ilya Petrov, Vladimir Guzov, Helisa Dharmo, Eduardo Pérez-Pellitero, and Gerard Pons-Moll. Force: Dataset and method for intuitive physics guided human-object interaction. *arXiv preprint arXiv:2403.11237*, 2024. 3

- [126] Xinming Zhang, Xianghui Wang, Lerong Zhang, Guodong Guo, Xiaoyu Shen, and Wei Zhang. Achieving stable high-speed locomotion for humanoid robots with deep reinforcement learning. *arXiv preprint arXiv:2409.16611*, 2024. [1](#)
- [127] Yunbo Zhang, Deepak Gopinath, Yuting Ye, Jessica Hodgins, Greg Turk, and Jungdam Won. Simulation and re-targeting of complex multi-character interactions. In *ACM SIGGRAPH 2023 Conference Proceedings*, pages 1–11, 2023. [15](#)
- [128] Chengfeng Zhao, Juze Zhang, Jiashen Du, Ziwei Shan, Junye Wang, Jingyi Yu, Jingya Wang, and Lan Xu. I’m hoi: Inertia-aware monocular capture of 3d human-object interactions. In *Proceedings of the IEEE/CVF Conference on Computer Vision and Pattern Recognition*, pages 729–741, 2024. [3](#)
- [129] Tony Z Zhao, Vikash Kumar, Sergey Levine, and Chelsea Finn. Learning fine-grained bimanual manipulation with low-cost hardware. *arXiv preprint arXiv:2304.13705*, 2023. [2](#), [5](#), [6](#), [7](#), [15](#), [16](#), [20](#)
- [130] Yuke Zhu, Josiah Wong, Ajay Mandlekar, Roberto Martín-Martín, Abhishek Joshi, Soroush Nasiriany, and Yifeng Zhu. robosuite: A modular simulation framework and benchmark for robot learning. *arXiv preprint arXiv:2009.12293*, 2020. [2](#), [4](#)
- [131] Ziwen Zhuang, Shenzhe Yao, and Hang Zhao. Humanoid parkour learning. *arXiv preprint arXiv:2406.10759*, 2024. [1](#)

Appendix

Contents:

- **A.** Additional Related Work
- **B.** Supplementary Experiments on Motion Tracking and Imitation Learning
- **C.** Details on Simulation Environment Configurations
- **D.** Details on Mimicking-Bench Task Evaluation Metrics
- **E.** Details on Motion Retargeting Algorithms
- **F.** Motion Tracking Algorithm Designs
- **G.** Imitation Learning Algorithm Designs
- **H.** Skill Learning Visualizations

A. Additional Related Work

A.1. Human-to-Humanoid Skill Transfer

Transferring skills from humans to humanoid robots is a popular research topic that guides humanoids to fulfill tasks in human-like manners. For locomotion skill learning, existing works [12, 81] integrate motion capture and synthetic human data as we do and adopt imitation learning on these data. To learn upper-body manipulation skills, previous studies [48, 56, 85, 117] propose learning from humanoid skill demonstrations collected by manual teleoperation due to the lack of relevant dataset support. Focusing on whole-body manipulation, a recent advance [24] presents a full-stack skill transfer pipeline combining retargeting, tracking, and imitation learning, supporting learning from real-time human teleoperation data.

A.2. Humanoid Motion Tracking

As a core technical step for humanoids mimicking human data, humanoid motion tracking aims at controlling humanoid agents to mimic animations and generate physically realistic motions. As technical foundations, several methodologies focus on tracking small-scale animation clips from specific locomotion [25, 76, 83], manipulation [10, 69], or multi-agent interaction [127] tasks using RL [10, 25, 69, 76, 115, 127] or differential simulators [83]. Benefiting from large diversities of motion tasks in recent datasets [40, 64, 104], an emerging research topic is to learn universal trackers [31, 61, 86, 103] that excel in tracking versatile tasks simultaneously, which encompasses two main challenges: how to generalize the trackers to novel motions [14, 86], and how to integrate tracking skills of numerous tasks into a single model [101, 107]. As solutions to the first challenge, most existing works leverage only general reward functions (e.g., humanoid joint position rewards [24, 36, 50, 60–62, 97, 112], task-agnostic contact graph rewards [103, 104]) suitable for diverse motions and tasks. To handle the second challenge, a line of work [66, 98, 101, 107] designs mixture-of-experts policies that first train specialist models to track different

types of tasks respectively and then distill them to a generalist, PHC [61] and PHC+ [62] propose active curriculum learning for hardly tracked animations, and VMP [86] learns motion priors covering versatile tasks and incorporates them into RL training process. With a growing demand for real-time teleoperating humanoids with sparse sensors [13, 36, 48, 85, 117], several recent works study tracking the animations of sparse humanoid key joints using teacher-student learning [35, 62, 96] or curriculum learning [21] paradigms.

B. Supplementary Experiments on Motion Tracking and Imitation Learning

In the main paper, we benchmark two motion tracking algorithms (Simplified PHC [61] and Improved HST [24]) and two imitation learning methods (HIT [24] and ACT [129]). This section presents evaluations of several additional algorithm designs with relatively unsatisfactory performances. Section B.1 examines the original HST [3], Section B.2 evaluates two additional imitation learning methods: Behavior Cloning (BC) [1] and Diffusion Policy [16], and Section B.3 reveals the data scaling law on human reference data scale for the performance improvement.

B.1. Motion Tracking

The original HST shares the same proprioception representations and training strategies with the official implementation of HumanPlus [3]. Table 9 compares its performance with the two algorithms presented in the main paper, indicating the original HST gets significant performance drops on most tasks. The reason is that the proprioception representation of the original HST excludes t , R , \bar{t} , and \bar{R} mentioned in Section F.1 that reflect task-space joint differences, leading to missing capability of rectifying cumulative tracking errors in joints’ global position and orientation. The task touching point (T) excludes navigation sensitive to cumulative errors, therefore the original HST achieves larger success rates on this task than on navigation-intensive SC, SS, LB, and LS.

Method	Motion Tracking Performance						
	SC	SS	LB	LS	T	L	Mean
Original HST [3]	0/0	1/1	0/0	4/2	28/13	0/0	5/3
Simplified PHC [61]	87/65	92/83	63/49	80/61	8/6	0/0	55/44
Improved HST [24]	92/70	90/89	88/82	55/53	58/40	25/20	68/59

Table 9. Task success rates (%) for different motion tracking methods. The retargeting algorithm is Optimization.

B.2. Imitation Learning

Behavior Cloning (BC) shares the same input and output representations with ACT, while its model is replaced

with CNN-MLP architecture, which is also implemented in ACT [1]. Diffusion policy [16] is a popular method taking multiple history frames information as a part of input and learning a diffusion model to recover actions from noises conditioned on input information. Both of them are single-stage methods that directly output 19 DoF action vectors. Table 10 compares their performances in task LB with the two imitation algorithms presented in the main paper, demonstrating their performances are limited in the vision-based mimicking pipeline. The reason for BC’s performance is that the underlying model architecture is not as powerful as transformers in ACT to process the relations between various input modalities. For diffusion policy, one observation is that the policy is likely to give commands to complete tasks before the humanoid actually reaches a proper position for interaction. A possible reason is that the denoised action vector in each diffusion step is dominated by the noisy action vector, which does not fully take advantage of visual observation conditions.

Method	Imitation Learning Performance
Behavior Cloning [1]	27/27
Diffusion Policy [16]	7/7
HIT [24]	36/34
ACT [129]	61/61

Table 10. Task success rates (%) for different imitation learning methods on task LB. The retargeting algorithm is Optimization and the motion tracking algorithm is the Improved HST.

B.3. Data Scaling Law

Section 5.6 in the main paper shows the significance of large-scale human references for imitation learning. We further compare the overall performance improvement of imitation learning policies trained on the human references of four different scales in task LB. We uncover that both kinematic and energy-averaged success rates keep an ascending trend approximately linear to the logarithm of the growing training data scale, shown in Figure 6.

C. Details on Simulation Environment Configurations

Section 3.1 in the main paper introduces our design of the simulation environment. It serves as a comprehensive platform across all six tasks to support reasonable task settings for the evaluation of the humanoid’s performance on various tasks. This section supplements details on the scene configuration (Section C.1) and the setting related to visual observation (Section C.2), as shown in Figure 7.

C.1. Scene Configuration

Initial scene layout: In each simulation environment, one object with one of its corresponding motion sequences

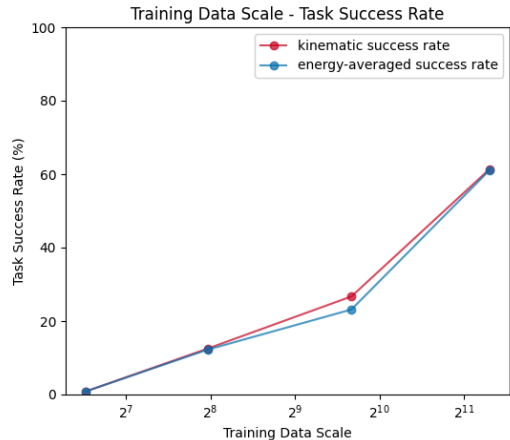


Figure 6. The ascending trend of task success rates on growing training data scale.

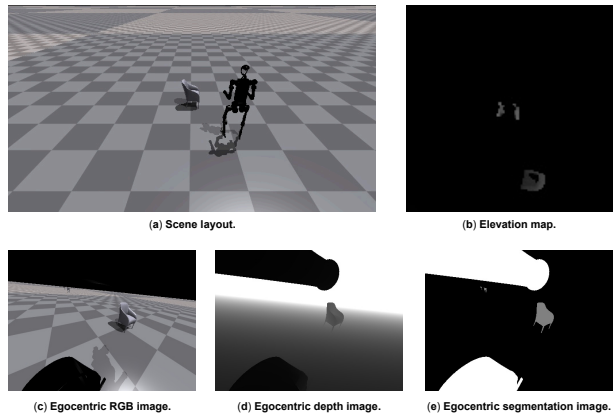


Figure 7. Mimicking-Bench simulation environment configurations. (a) exemplifies an initial scene layout for task SC. (b) shows the captured elevation map \mathcal{E} in the scene. (c) (d) and (e) show the RGB image \mathcal{C} , depth image \mathcal{D} and segmentation image \mathcal{S} captured by the left front camera in the scene, respectively.

is randomly sampled from the test set mentioned in Section 5 in the main paper. The object is posed canonically at the origin of the scene and oriented towards the positive X -axis. The humanoid’s initial pose is set to the pose in the first frame of the sampled motion sequence. For tasks SC, SS, LB, and LS that demand locating and navigating, to avoid the humanoid being too far away from the object to detect it visually, we further normalize the humanoid’s initial positions beyond the range of visual detection, clipping their distances to the origin within 2m.

Time limit: For tasks T and L, the time limit for the robot to complete the task is set to 10s. For tasks SC, SS, LB, and LS, the time limit is set to 20s, considering additional time cost on necessary relatively long-distance movement.

C.2. Egocentric Camera Setup and Visual Observation

For each camera in all tasks, the resolution is set to 360×480 with a 120-degree field of view. The methods of obtaining visual observations of the two modalities are described below.

Camera setup for tasks SC, SS, LB, and LS: These tasks involve complex spatial relations between the humanoid’s whole body and objects. Hence in these tasks, four cameras are uniformly attached around the humanoid’s pelvis and respectively set to face right front, left front, left back, and right back, all with a 35° downward pitch. This camera configuration enables the humanoid to capture the whole surrounding environment in a 360-degree view, providing necessary self-positioning information for further planning.

Camera setup for tasks T and L: These tasks require precise hand motions, while their humanoid-object spatial relations are relatively simple since the humanoid initially stands in front of the object. To adapt to such requirements, we reduce the number of cameras to one to capture objects at relatively fixed positions in front of the humanoid. We locate this camera 0.55m above the pelvis and orient it to face forward with 55° downward pitch, aggregating the information of arms and hands into visual inputs.

Multi-view RGB, depth and segmentation images: In each frame, cameras return RGB images \mathcal{C} , depth images \mathcal{D} and segmentation images \mathcal{S} , with depth values clipped to 50m. For task touching points (T), two task target hand points are projected onto RGB images, and the projected image pixels are colored red.

Elevation map: For visual observation \mathcal{E} , elevation maps [70] are computed from raw depth images by two steps. Depth images \mathcal{D} are first filtered out depth values larger than 6m and remaining values are converted into point clouds $\mathcal{P}_{\text{root}}$ in the local coordinate of humanoid’s root joint. Then the points in $\mathcal{P}_{\text{root}}$ are projected into uniform 2D square grids divided on the horizontal plane surrounding the humanoid. The resolution of 2D grids is 128×128 and each grid corresponds to a pixel in the final elevation map. For each grid g , the corresponding pixel value in the elevation map is the maximum height of points in $\mathcal{P}_{\text{root}}$ that are projected into g :

$$\mathcal{E}(g) = \max \{p_z | p \in \mathcal{P}_{\text{root}}, \text{proj}(p) \in g\} \quad (1)$$

The final elevation map \mathcal{E} is a grayscale map of resolution 128×128 representing the surrounding scene height information. The humanoid is located at the center and facing downward in the elevation map. For tasks except T, the grid size is $4\text{cm} \times 4\text{cm}$. For task T, the grid size is designed as $1\text{cm} \times 1\text{cm}$ for more accurate target instruction. Besides, an additional target point elevation map $\mathcal{E}_{\text{target}}$ is provided

for goal instruction, as a black image only highlighting the heights and relative positions of two target points.

D. Details on Mimicking-Bench Task Evaluation Metrics

Section 3.2 in the main paper mentions that we design the task-specific kinematic evaluation metric K and the task-agnostic physical metric P to examine whether a humanoid motion fulfills the task. A motion is treated as successful only if it achieves K and P simultaneously. This section presents details on the kinematic metrics for each task (Section D.1) and hyperparameters for the physical evaluation metric (Section D.2), respectively.

D.1. Kinematic Evaluation Metric

(1) Sitting on a Chair (SC): K evaluates whether the pelvis of the humanoid keeps above the seat surface for 0.3 seconds. In each frame, the pelvis is above the seat surface only if the root position of the humanoid lies in the chair’s interior in the bird-eye view, and its height lies in $[H, H + 0.27\text{m}]$, where H is the height of the seat.

(2) Sitting on a Sofa (SS): K is the same as that for SC.

(3) Lying on a Bed (LB): K evaluates whether the pelvis and ankles of the humanoid keep on the bed for 0.3 seconds. In each frame, a humanoid joint is on the bed only if its position lies in the bed’s interior in the bird-eye view, and its height lies in $[H, H + 0.4\text{m}]$, where H is the height of the bed’s seat.

(4) Lying on a Sofa (LS): K evaluates whether the pelvis keeps on the sofa meanwhile the ankles keep above half of the sofa’s height for 0.3 seconds. In each frame, the pelvis is on the sofa only if the humanoid’s root position lies in the sofa’s interior in the bird-eye view, and its height lies in $[H, H + 0.4\text{m}]$, where H is the height of the sofa’s seat.

(5) Touching Points near an Object (T): K evaluates whether the two wrists keep within 0.1m of their target positions in 1 second.

(6) Lifting a Box (L): K evaluates whether the box is lifted 0.2m high meanwhile the two wrists are within 0.1m of the box surface in the last frame.

D.2. Hyperparameters on Physical Evaluation Metric

The physical metric $P = [\max(\|\tau_i v_i\|^2) < \lambda_P]$ evaluates whether the humanoid can keep moving with low energy cost. Due to the unknown expected value of λ_P for real-world deployment, we empirically set λ_P as $1\text{e}6$, $2\text{e}6$, $4\text{e}6$, and $8\text{e}6$, and report the average success rates on evaluating under these four values.

E. Details on Motion Retargeting Algorithms

Motion retargeting is the first step of the skill-learning paradigm, which aims to transfer motion animations from human skeletons to humanoid ones. We benchmark three types of motion retargeting algorithms: copy-rotation, optimization, and optimization with skeleton shape alignment. This section presents details on human-to-humanoid joint mapping (Section E.1), optimization (Section E.2), and skeleton shape alignment (Section E.3).

E.1. Human-to-Humanoid Joint Mapping

The human-to-humanoid joint mapping M builds joint-wise correspondences between the two skeletons. We provide the mapping for the three human models from UniHSI [108], ROAM [122], and CORE4D [118] in Table 11, 12, and 13, respectively. Given the joint mapping, the copy-rotation algorithm directly copies joint rotations from human to humanoid.

UniHSI [108] Human Skeleton		H1 Humanoid Skeleton	
Joint Index	Semantics	Joint Index	Semantics
0	pelvis	0	pelvis
0	pelvis	11	torso
12	left hip	1	left hip yaw
12	left hip	2	left hip row
13	left knee	4	left knee
14	left ankle	5	left ankle
9	right hip	6	right hip yaw
9	right hip	7	right hip row
10	right knee	9	right knee
11	right ankle	10	right ankle
6	left shoulder	13	left shoulder row
7	left elbow	15	left elbow
3	right shoulder	17	right shoulder row
4	right elbow	19	right elbow

Table 11. Joint mapping between UniHSI [108] human model and H1.

ROAM [122] Human Skeleton		H1 Humanoid Skeleton	
Joint Index	Semantics	Joint Index	Semantics
0	pelvis	0	pelvis
0	pelvis	11	torso
17	left hip	1	left hip yaw
17	left hip	2	left hip row
18	left knee	4	left knee
19	left ankle	5	left ankle
22	right hip	6	right hip yaw
22	right hip	7	right hip row
23	right knee	9	right knee
24	right ankle	10	right ankle
10	left shoulder	12	left shoulder pitch
11	left elbow	15	left elbow
14	right shoulder	16	right shoulder pitch
15	right elbow	19	right elbow

Table 12. Joint mapping between ROAM [122] human model and H1.

CORE4D [118] Human Skeleton		H1 Humanoid Skeleton	
Joint Index	Semantics	Joint Index	Semantics
0	pelvis	0	pelvis
0	pelvis	11	torso
1	left hip	1	left hip yaw
1	left hip	2	left hip row
4	left knee	4	left knee
7	left ankle	5	left ankle
2	right hip	6	right hip yaw
2	right hip	7	right hip row
5	right knee	9	right knee
8	right ankle	10	right ankle
16	left shoulder	12	left shoulder pitch
18	left elbow	15	left elbow
17	right shoulder	16	right shoulder pitch
19	right elbow	19	right elbow

Table 13. Joint mapping between CORE4D [118] human model and H1.

E.2. Details on Optimization

In the optimization algorithm, the state is the humanoid motion configuration $M = \{R \in \mathbb{R}^{T \times 3}, t \in \mathbb{R}^{T \times 3}, J \in \mathbb{R}^{T \times 19}\}$, where T is the frame number, R is root global orientations, t is root global positions, and J is joint angles. We find the optimal state M^* that minimizes the following loss function:

$$\mathcal{L}_{\text{optim}} = \lambda_{\text{pos}} \mathcal{L}_{\text{pos}} + \lambda_{\text{hand}} \mathcal{L}_{\text{hand}} + \lambda_{\text{ori}} \mathcal{L}_{\text{ori}} + \lambda_{\text{acc}} \mathcal{L}_{\text{acc}}, \quad (2)$$

where \mathcal{L}_{pos} is the mean-square error between global positions of human and humanoid corresponding joints, $\mathcal{L}_{\text{hand}}$ is the above error between human and humanoid wrists and only applies to tasks T and L, \mathcal{L}_{ori} is the mean absolute geodesic distance between global orientations of human and humanoid corresponding joints, and \mathcal{L}_{acc} is the mean absolute acceleration of J adopted to improve motion smoothness. λ are hyperparameters.

The optimization is conducted by an Adam optimizer with a learning rate of 0.02 and 3000 epochs.

E.3. Details on Motion Retargeting Algorithms

OmniH2O [35] proposes to find optimal SMPL-X [74] shape parameters making the human skeleton best aligned with that of H1 in the T-pose. This strategy is equivalent to adjusting human bone lengths to fit those of H1 for an arbitrary human skeleton [93]. We thus combine this strategy with the previous optimization as another type of retargeting algorithm. In practice, this strategy fits human joint global orientations and root’s global position and modifies bone lengths to update human joint positions in each frame. We denote this algorithm as OmniH2O [35] in experiments.

F. Motion Tracking Algorithm Designs

Given retargeted humanoid-scene interaction animations, motion tracking aims to track the animations in the simulation environment and obtain physically realistic motions as skill demonstrations. We benchmark two existing RL-based trackers, simplified PHC [61] and improved HST [24], and present their key technical designs in this section.

F.1. Input

The tracker’s input consists of proprioceptions S of the current humanoid and the animation target of the next frame. For task touching points (T), the input also includes the wrists’ position target in the current humanoid root’s coordinate system. For task lifting a box (L), the input also includes states (i.e., 3D position, 3D orientation, 3D linear velocity, and 3D angular velocity) of the current box and its animation target represented in the current humanoid root’s coordinate system. The proprioceptions for each tracker are defined below.

Improved HST: $S = \{J \in \mathbb{R}^{19}, \dot{J} \in \mathbb{R}^{19}, t \in \mathbb{R}^{20 \times 3}, R \in \mathbb{R}^{20 \times 3}, v \in \mathbb{R}^{20 \times 3}, \omega \in \mathbb{R}^{20 \times 3}, \bar{J} \in \mathbb{R}^{19}, \dot{\bar{J}} \in \mathbb{R}^{19}, \bar{t} \in \mathbb{R}^{20 \times 3}, \bar{R} \in \mathbb{R}^{20 \times 3}, \bar{v} \in \mathbb{R}^{20 \times 3}, \bar{\omega} \in \mathbb{R}^{20 \times 3}, \bar{a} \in \mathbb{R}^{19}, g \in \mathbb{R}^3\}$, where:

- J and \dot{J} are joint angles and velocities of the current humanoid.
- t , R , v , and ω are joints’ positions, orientations, linear velocities, and angular velocities of the current humanoid in the current humanoid’s root coordinate system.
- \bar{J} and $\dot{\bar{J}}$ are joint angles and velocities of the animation target.
- \bar{t} , \bar{R} , \bar{v} , and $\bar{\omega}$ are joints’ positions, orientations, linear velocities, and angular velocities of the animation target in the current humanoid’s root coordinate system.
- \bar{a} is the generated action vector in the last frame.
- g is the gravity direction in the current humanoid’s root coordinate system.

Simplified PHC: The S for this method is the combination of the S for the improved HST and $\{t - \bar{t}, R - \bar{R}\}$, which induce the tracker to learn from state differences explicitly.

F.2. Output

In each frame, the tracker’s output is a 19 DoF action vector representing joint angles. Joint torques are then computed via predefined PD gains and fed into the simulation environment to control the humanoid physically.

F.3. Reward Designs

We design task-specific reward functions due to significantly different focuses on different tasks. We provide reward designs for the improved HST below, while those for

the simplified PHC are mostly similar to them but exclude regularizers.

For tasks SC, SS, LB, and LS: The overall reward function is $r_{\text{overall}} = r_{\text{human}} + r_{\text{reg}}$, where:

- $r_{\text{human}} = r_{\text{pos}} + r_{\text{ori}} + r_{\text{root}}$ encourages tracker motions to approach animation targets, where $r_{\text{pos}} = \exp(-5 \sum_{i=1}^{20} \|t_i - \bar{t}_i\|_2^2)$ measures joint position error, $r_{\text{ori}} = \sum_{i=1}^{20} \exp(-\text{Geo}(R_i, \bar{R}_i))$ measures joint orientation error (“Geo” denotes the geodesic distance between the two rotation matrices), and $r_{\text{root}} = 5 \exp(-10 \|t_{\text{root}} - \bar{t}_{\text{root}}\|_1) - \lambda_{\text{height}} (\text{height}_{\text{root}} - \bar{\text{height}}_{\text{root}})^2$ emphasizes the root accuracy (“height” denotes the height of a joint in the world coordinate system, and λ_{height} is set to 100 for the two sitting tasks and 10 for others).
- $r_{\text{reg}} = r_{\text{action}} + r_{\text{vel}} + r_{\text{acc}} + r_{\text{energy}}$ is the regularizers penalizing motions with high speeds or energies, where $r_{\text{action}} = -1e - 3 \|a - \bar{a}\|_2^2$ penalizes action changes, $r_{\text{vel}} = -2e - 3 \|\dot{J} - \dot{\bar{J}}\|_2^2$ penalizes large joint velocities, $r_{\text{acc}} = -5e - 7 \|\ddot{J} - \ddot{\bar{J}}\|_2^2$ penalizes large joint accelerations, and $r_{\text{energy}} = 1e - 6 \|\tau \dot{J}\|_2^2$ penalizes large joint torques and velocities.

For task T: To further enhance wrist accuracy, the overall reward function is $r_{\text{overall}} = r_{\text{human}} \times r_{\text{wrist}} + r_{\text{reg}}$. r_{human} and r_{reg} are similar to those for the previous four tasks, while $r_{\text{wrist}} = \exp(-10 \|t_{\text{left wrist}} - \bar{t}_{\text{left wrist}}\|_1) + \exp(-10 \|t_{\text{right wrist}} - \bar{t}_{\text{right wrist}}\|_1)$ highlights wrist accuracy.

For task L: To better induce object moving, the overall reward function is $r_{\text{overall}} = r_{\text{human}} \times r_{w \rightarrow o} \times r_{\text{object}} + r_{\text{reg}}$. r_{human} and r_{reg} are similar to those for the previous five tasks. $r_{w \rightarrow o} = \exp(-10 \|(t_{\text{left wrist}} - t_{\text{object}}) - (\bar{t}_{\text{left wrist}} - \bar{t}_{\text{object}})\|_1) + \exp(-10 \|(t_{\text{right wrist}} - t_{\text{object}}) - (\bar{t}_{\text{right wrist}} - \bar{t}_{\text{object}})\|_1)$ encourages wrist positions relative to the object to get close to those of the animation target, and $r_{\text{object}} = \exp(-10 \|t_{\text{object}} - \bar{t}_{\text{object}}\|_1)$ encourages moving the object to approach its animation target. We observe that r_{human} , $r_{w \rightarrow o}$, and r_{object} are all indispensable for completing the task successfully.

F.4. Training Strategies

The two trackers both include the early-termination strategy [76] that terminates the rollout when the current humanoid root is 0.5m far from that of the animation target or its height is lower than a task-specific acceptance threshold. The basic RL algorithm is ActorCritic with PPO [84].

G. Imitation Learning Algorithm Designs

The physically realistic motions generated by trackers can be utilized as large-scale skill demonstrations for imitation learning. The imitation learning policy aims to imitate demonstration motions during training, and output control

commands to complete tasks based on proprioceptions and visual observations without any instructions from animation motions during evaluation. We benchmark two imitation learning algorithms, ACT [129] and HIT [24] as representatives of the single-stage and two-stage algorithms, respectively. And we present their design details in this section.

G.1. Input

Compared to the tracker’s input, the input of the imitation learning policy consists of proprioceptions and egocentric visual observations of the current humanoid, excluding any animation target information or direct object state information.

The definition of proprioception is the subset of S in the input of the corresponding tracker (Section F.1) that generates demonstration data. Specifically, we partition tracker’s proprioceptions S into two parts S_{current} and S_{target} , and only feed S_{current} into imitation learning policies:

- $S_{\text{current}} = \{J, \dot{J}, t, R, v, \omega, \tilde{a}, g\}$, which can be directly obtained in the simulation environment without animation targets.
- $S_{\text{target}} = \{\bar{J}, \dot{\bar{J}}, \bar{t}, \bar{R}, \bar{v}, \bar{\omega}\}$, which relies on animation targets.

Egocentric visual observations are $\mathcal{C} + \mathcal{D}$ as multi-view RGBD images or \mathcal{E} as elevation maps. For task touching points (T) using elevation map modality, additional target point elevation maps $\mathcal{E}_{\text{target}}$ are provided as goal instruction (Section C.2). Each visual observation is processed by image backbones to be further concatenated with proprioception inputs.

G.2. Output

The two imitation learning policies output commands for two different stages in humanoid control, which is one of the main distinctions between them. The outputs of each policy are defined below.

ACT: ACT is a single-stage algorithm and its imitation target is exactly the tracker’s output. Namely, ACT aims to output the same 19 DoF action vector as the tracker outputs.

HIT: HIT is a two-stage algorithm leveraging the corresponding tracker in inference. In the first stage of the algorithm, HIT predicts a high-level plan for target humanoid poses \hat{S}_{target} in the next frame, wrists’ position target if the task is touching points (T) and box states if the task is lifting a box (L). HIT’s outputs complement all required input information for its corresponding tracker and are concatenated to S_{current} as a tracker’s complete input \hat{S} . In the second stage, the low-level tracker takes \hat{S} and outputs the final 19 DoF action vector to physically execute the predicted plan.

Since S_{target} is in high dimension and can be recovered by its subset, instead of directly imitating it, we design HIT’s imitation target of S_{target} to be the subset $\{\bar{J} \in \mathbb{R}^{19}, \dot{\bar{J}} \in$

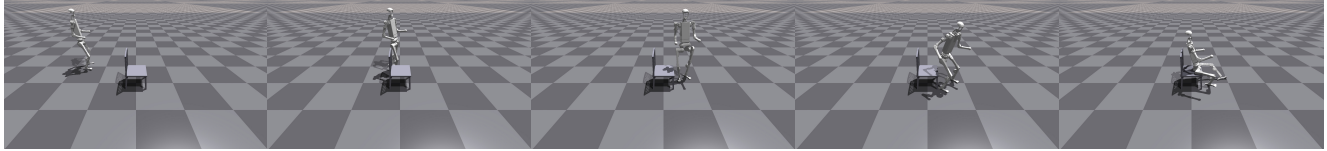
$\mathbb{R}^{19}, \bar{t}_{\text{root}} \in \mathbb{R}^3, \bar{R}_{\text{root}} \in \mathbb{R}^6\}$, where $\bar{t}_{\text{root}}, \bar{R}_{\text{root}}$ are the root joint’s position and orientation of the future humanoid in the current humanoid’s root coordinate system. To recover the root velocity information, HIT predicts for the next two frames instead of the next single frame. Then all information in S_{target} can be recovered by taking the temporal difference between two frames and computing forward kinematics.

G.3. Training Strategies

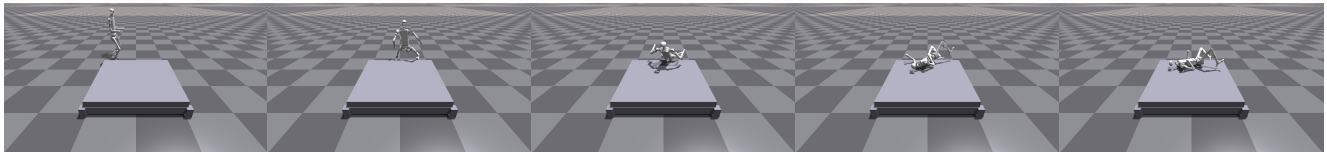
The training of the two imitation learning policies includes predictions for a future chunk instead of a single future frame to supervise the imitated control for a longer horizon. During training, HIT also supervises the difference in image embeddings between the prediction and the ground truth in a future chunk. During inference, these auxiliary supervision channels are ignored and only the predicted action in the first following frame is utilized for more precise control.

H. Skill Learning Visualizations

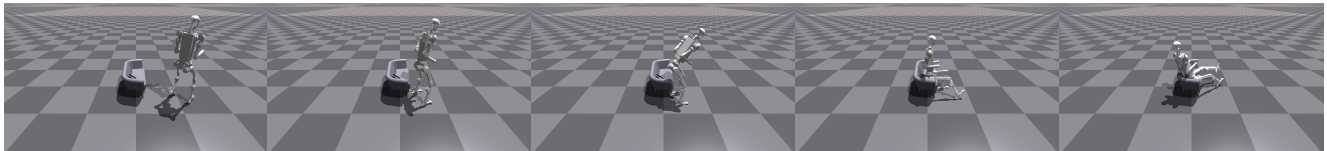
Figure 8 exemplifies learned humanoid-scene interaction skills for each task. More visualizations are provided in our video.



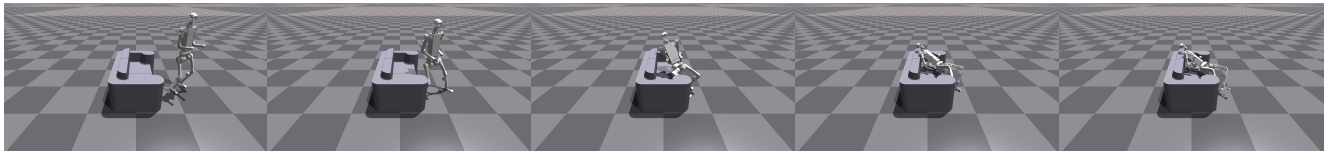
(a) IL performance on task *Sit Chair*



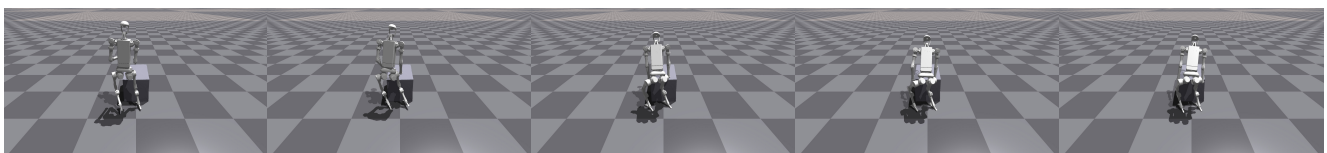
(b) IL performance on task *Lie Bed*



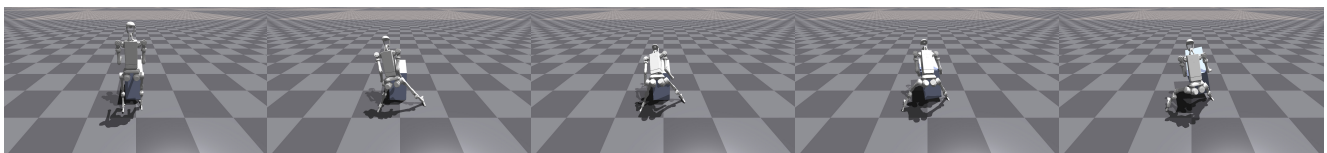
(c) IL performance on task *Sit Sofa*



(d) IL performance on task *Lie Sofa*



(e) IL performance on task *Touch Point*



(f) IL performance on task *Lift Box*

Figure 8. **Examples of imitation learning performance on various tasks.** The retargeting, tracking, and imitation learning algorithms are Optimization, Improved HST, and ACT, respectively.